

A New Modeling Approach for Planar Beams: Finite-Element Solutions based on Mixed Variational Derivations

Ferdinando Auricchio^{*a,b,c,d}, Giuseppe Balduzzi^{a,e}, Carlo Lovadina^{c,d,e}

May 31, 2010

^a Dipartimento di Meccanica Strutturale (DMS), Università degli Studi di Pavia,
via Ferrata 1, 27100 Pavia Italy

^b European Centre for Training and Research in Earthquake Engineering (EUCENTRE), Pavia, Italy

^c Istituto di Matematica Applicata e Tecnologie Informatiche (IMATI), CNR, Pavia, Italy

^d Centro di Simulazione Numerica Avanzata (CeSNA), IUSS, Pavia, Italy

^e Dipartimento di Matematica “Felice Casorati”, Università degli Studi di Pavia,
via Ferrata 1, 27100 Pavia Italy

Abstract

This paper illustrates a new modeling approach for planar linear elastic beams. Referring to existing models, we first introduce the variational principles that could be adopted for the beam model derivation, discussing their relative advantages and disadvantages. Then, starting from the Hellinger-Reissner functional we derive some homogeneous and multilayered beam models, discussing some properties of their analytical solution. Finally, we develop a planar beam finite element, following an innovative approach that could be seen as the imposition of equilibrium in the cross-section and compatibility along the axis. The homogeneous model is capable to reproduce the behavior of Timoshenko beam, with the advantage that the shear correction factor appears naturally from the variational derivation; the multilayered beam is capable to capture the local effects produced by boundary constraints and load distributions; the finite element is capable to predict the cross-section stress distribution with high accuracy, and more generally the behavior of planar structural elements.

Keyword: laminated linear elastic beam; analytical solution; finite element modelling; mixed variational formulation.

1 Introduction

To reproduce the mechanical behavior of structural elements characterized by one dimension predominant with respect to the other two (i.e. a beam) the most classical approaches are the well-known Euler Bernoulli (shortly EB) and Timoshenko theories illustrated in standard literature (e.g. see Timoshenko (1955) and Hjelmstad (2005)). Generally adopted for very slender elements, the EB beam model assumes cross-section axial and transverse displacements as one dimensional unknown fields, converting the 3D elastic problem, formulated through a set of partial differential equations (PDE), into a simpler system of two ordinary differential equations (ODE). On the other hand, adopted for less slender structural elements, Timoshenko beam model assumes cross-section axial and transverse displacements, together with rotations as one-dimensional fields, leading to a set of three ODE. As a consequence of the field assumptions, these models are often cited in literature as *first-order* models. Moreover, we denote these models as *displacement-based*

*Email address: auricchio@unipv.it

to underline that usually these models consider only displacements as independent variables and stresses are evaluated by post processing.

Despite their simplicity (also related to the possibility of computing analytical solutions) and their excellent first-design ability, EB and Timoshenko models have some well-known limitations, which we wish to cite:

- loss of accuracy for beams with low ratio between length and cross-section characteristic dimension,
- loss of accuracy in modeling non-homogeneous beams (such as composites) as well as in modeling non-linear material behavior,
- difficulty in computing accurate stress profiles, connected to the fact that only mean-value displacements are assumed as field variables.

Hence, due to the need of more accurate one-dimensional models, researchers have developed new approaches that can generally be classified as:

- **high-order, displacement-based models**, which introduce more sophisticated cross-section kinematics,
- **mixed or hybrid models**, which introduce also stresses – and sometimes even strains – as independent variables.

Just to give a few examples, an often cited model falling in the first category is the one proposed by Reddy (1984) that introduces section warping in addition to Timoshenko displacements. As discussed by Sheinman (2001), this model shows an inconsistency, since transverse displacement generates a constant cross-section shear distribution, whereas axial displacements give a quadratic one. A more complete kinematics is adopted in the model proposed by Lo et al. (1977a) where, considering both section warping and striction, authors eliminate such an inconsistency. For a general treatment of high-order, planar, kinematic beam models and discussion of their analytical solutions the readers may refer to the work of Sheinman (2001).

With respect to mixed models, a very interesting approach is the one proposed by Alessandrini et al. (1999), where, starting from 3D elasticity, the authors illustrate a clear derivation of some plate models, studying also the convergence of the models under consideration.

As far as the numerical modeling is concerned, a literature review shows that the number of proposed finite element (FE) implementations is nearly uncountable. This also depends on the fact that many different choices are possible depending on:

- **functional formulation and independent variables**: the simplest functionals consider only kinematic variables, as in the displacement based beam models while, on the contrary, the most complicated ones consider also stresses and strains;
- **order of field approximation**: in addition to the first- versus high-order classification, for the case of multilayered beams, *layer-wise* models adopt piecewise layer-defined functions while *global* models use globally defined functions to describe the field distribution on cross-section.

For both items, intermediate choices are possible, e.g. only some stress components could be selected as independent variables, or some fields are described layer-wise, while the remaining ones are assumed as global functions.

It is interesting to observe that in available review-papers (e.g., see Carrera (2000) and Wanji and Zhen (2008)), the authors usually compare the developed models by considering different field approximations but derived from the same principle. Therefore, it is possible to understand only the effect of basis accuracy, but not the improvements introduced considering a more sophisticated variational principle. With this respect, in Section 3 we present different variational principles that can be employed, briefly discussing their respective features and possible drawbacks.

The main aim of this paper is to propose a simple analytical model and a FE capable of capturing the section stress distribution with high accuracy, also in a multilayered body. We opt for the *dimension reduction variational* approach, classical in beam modeling, and used among others by Alessandrini et al. (1999) for plate problems. This method could allow to generalize the model to other more complex situations, such as non linear constitutive laws, for instance.

A summary of the paper is as follows. In Section 2 we define the problem we are going to tackle, in Section 3 we introduce the functionals which may be used for the model derivation, listing for each one properties and developed models presented in the literature; by means of this discussion we are able to choose an appropriate variational principle as the starting point for the model derivations. In Sections 4 we derive some 1D models, while in Section 5 we present a few examples, giving some insight on the structure of the corresponding analytical solution. In Section 6 we develop suitable finite element schemes, and we present some results to illustrate their actual computational performances.

2 Problem definition

The object of our study is a planar beam Ω , not necessarily homogeneous along the thickness and modeled as a 2D body: this is equivalent to impose plane stress state hypotheses to a three-dimensional body or to state that the beam width is negligible. Moreover, we limit the discussion to linear elastic isotropic materials and small displacements.

We define the problem domain as:

$$\Omega = l \times A$$

where the beam longitudinal axis l and the cross-section A are defined as:

$$l = \{x \in \mathbb{R} \mid x \in [0, \bar{l}]\} \quad A = \left\{y \in \mathbb{R} \mid y \in \left[-\frac{h}{2}, \frac{h}{2}\right]\right\}$$

in which h is the beam thickness and \bar{l} is the beam length.

Obviously $\bar{l} \gg h$ so that the longitudinal axis is the predominant dimension of the body. Figure 1 represents the domain and the adopted Cartesian coordinate system.

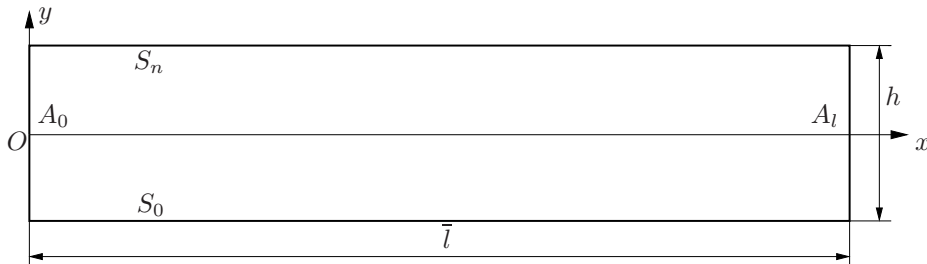


Figure 1: Planar beam geometry, coordinate system, dimensions and adopted notations.

As illustrated in Figure 1 we define the lateral cross-sections as A_0 and A_l , while the bottom and upper boundaries as S_0 and S_n , respectively. We denote the domain boundary as $\partial\Omega$, so that $\partial\Omega = (A_0 \cup A_l) \cup (S_0 \cup S_n)$. For $\partial\Omega$, we consider the partition $\{\partial\Omega_t; \partial\Omega_s\}$, where $\partial\Omega_t$ and $\partial\Omega_s$ are the externally loaded and the displacement constrained boundaries, respectively. The external load is defined as a line force density $\mathbf{t} : \partial\Omega_t \rightarrow \mathbb{R}^2$ whereas the body load is defined as an area force density $\mathbf{f} : \Omega \rightarrow \mathbb{R}^2$; moreover we specify a sufficiently smooth boundary displacement function $\bar{\mathbf{s}} : \partial\Omega_s \rightarrow \mathbb{R}^2$. Finally, we suppose that the beam is made by layers whose thickness is constant along the axial coordinate x , but not necessarily the same at each layer. Consequently, the Young's modulus E and the Poisson's ratio ν are scalar fields depending on the thickness coordinate y , i.e. $E : A \rightarrow \mathbb{R}$ and $\nu : A \rightarrow \mathbb{R}$.

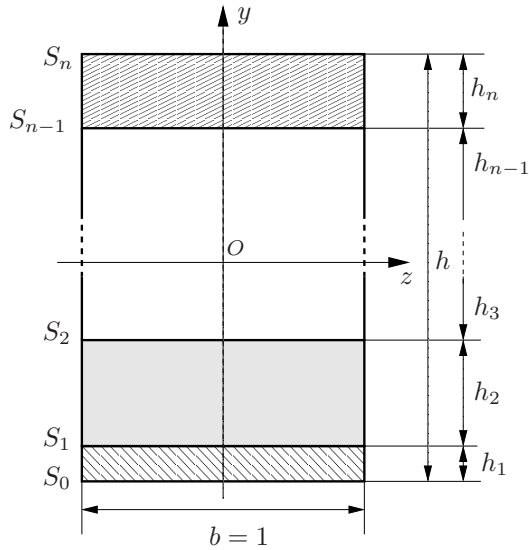


Figure 2: Cross-section geometry, coordinate system, dimensions and adopted notations.

Introducing the following independent variable fields:

$$\boldsymbol{\sigma} : \Omega \rightarrow \mathbb{R}^{2 \times 2} \quad \boldsymbol{\varepsilon} : \Omega \rightarrow \mathbb{R}^{2 \times 2} \quad \mathbf{s} : \Omega \rightarrow \mathbb{R}^2$$

where the stress $\boldsymbol{\sigma}$ and the strain $\boldsymbol{\varepsilon}$ are symmetric tensors while the displacement \mathbf{s} is a vector, the strong formulation of the problem under investigation corresponds to the following boundary value problem:

$$\begin{cases} \boldsymbol{\varepsilon} = \nabla^s \mathbf{s} & (1a) \\ \boldsymbol{\sigma} = \mathbf{D} : \boldsymbol{\varepsilon} & (1b) \\ \nabla \cdot \boldsymbol{\sigma} + \mathbf{f} = \mathbf{0} & (1c) \end{cases} \quad \text{in } \Omega$$

$$\boldsymbol{\sigma} \cdot \mathbf{n} = \mathbf{t} \quad \text{on } \partial\Omega_t \quad (1d)$$

$$\mathbf{s} = \bar{\mathbf{s}} \quad \text{on } \partial\Omega_s \quad (1e)$$

where Equation (1a) is the compatibility relation, Equation (1b) is the material constitutive relation in which \mathbf{D} is the appropriate fourth order linear elastic tensor and Equation (1c) represents the equilibrium condition. Equations (1d) and (1e) are the boundary equilibrium and the boundary compatibility condition, respectively.

3 Variational problem formulations and modeling methods

In this section we are going to present different possible variational formulations for Problem (1). In particular, we introduce approaches based on total potential energy, Hellinger-Reissner and Hu-Washizu functionals, considering for each one different possible stationarity conditions. Restricting to the framework of Section 2, we emphasize that a variational beam model can be considered as the outcome of the following general procedure.

- **First step.** A variational principle is selected for the 2D planar elasticity problem. In particular, the functional spaces for the involved fields has to be appropriately chosen.

- **Second step.** For each involved field, an approximation profile is selected. Typically, to develop a beam model, one chooses polynomial or piecewise polynomial shapes along the thickness direction, while no profile restrictions are imposed along the axial direction. However, the approximation fields should fit the functional framework of the **First step** above, at least if a *conforming* model is considered.
- **Third step.** Integration along the thickness direction is performed. This way, the 2D variational problem is reduced to a 1D variational problem, which corresponds to a system of ODEs equipped with boundary conditions (i.e. the beam model).

3.1 Total Potential Energy approach

Total Potential Energy (shortly TPE) is the functional most frequently used in continuum mechanics and in standard literature (e.g. Hjelmstad, 2005); several authors use it as a starting point to derive both first-order beam models as well as the most popular corresponding FE formulations.

The TPE functional can be expressed as follows:

$$J_{TPE}(\mathbf{s}) = \frac{1}{2} \int_{\Omega} \nabla^s \mathbf{s} : \mathbf{D} : \nabla^s \mathbf{s} d\Omega - \int_{\Omega} \mathbf{s} \cdot \mathbf{f} d\Omega \quad (2)$$

Boundary conditions will be suitably imposed in what follows. The critical point of the functional above corresponds to find the energy minimizer, which is unique and stable in the usual framework of admissible displacement space.

Requiring stationarity of TPE (2), we obtain the following weak problem:

Find $\mathbf{s} \in W^s$ such that $\forall \delta \mathbf{s} \in \overline{W}^s$:

$$\delta J_{TPE}^s = \int_{\Omega} \nabla^s (\delta \mathbf{s}) : \mathbf{D} : \nabla^s \mathbf{s} d\Omega - \int_{\Omega} \delta \mathbf{s} \cdot \mathbf{f} d\Omega - \int_{\partial\Omega_t} \delta \mathbf{s} \cdot \mathbf{t} dS = 0 \quad (3)$$

where

$$W^s := \{ \mathbf{s} \in H^1(\Omega) : \mathbf{s}|_{\partial\Omega_s} = \overline{\mathbf{s}} \} \quad \overline{W}^s := \{ \delta \mathbf{s} \in H^1(\Omega) : \delta \mathbf{s}|_{\partial\Omega_s} = \mathbf{0} \}$$

We define Equation (3) as the **TPE symmetric stationarity** that is often used as a basis for FE development, leading obviously to a symmetric stiffness matrix.

Wanji and Zhen (2008) give a review on multilayered, elastic, displacement-based (i.e., TPE derived) plate FE. Increasing orders of field approximation are considered, from the simplest model in which displacements are globally defined along the cross-section, to the most sophisticated ones in which displacements are defined layer-wise. Wanji and Zhen also notice that almost all the presented FE perform only for some specific problems (thick laminated plates, soft-core sandwich, etc.), but they are not able to accurately describe the shear distribution along the thickness in the general case.

An accurate evaluation of shear distribution is one of the aims of the work by Vinayak et al. (1996a,b), in which the authors develop a multilayered planar beam FE starting from Equation (3), using the field approximation proposed by Lo et al. (1977a,b) and appropriately treating the thickness heterogeneity. They propose two ways to evaluate the axial and transverse stresses: the first one uses the compatibility and the constitutive relations (Equations (1a) and (1b)), while the second one refines the shear and the out-of-plane stress distributions using the equilibrium relation (1c). The resulting numerical schemes are generally satisfactory, but the computed solutions might exhibit instabilities near the boundary, and the stress distributions are not always sufficiently accurate.

As a general remark (see Rohwer and Rolfes (1998) and Rohwer et al. (2005)), in TPE-based models the critical step is the post processing stress evaluation that could compromise the effectiveness of the method.

3.2 Hellinger-Reissner approach

The Hellinger-Reissner (shortly HR) functional can be expressed as:

$$J_{HR}(\boldsymbol{\sigma}, \mathbf{s}) = \int_{\Omega} \boldsymbol{\sigma} : \nabla^s \mathbf{s} \, d\Omega - \frac{1}{2} \int_{\Omega} \boldsymbol{\sigma} : \mathbf{D}^{-1} : \boldsymbol{\sigma} \, d\Omega - \int_{\Omega} \mathbf{s} \cdot \mathbf{f} \, d\Omega \quad (4)$$

How boundary conditions will be enforced depends on the specific variational formulation employed to express the stationarity of the functional (cf. Sections 3.2.1 and 3.2.2). We also wish to remark that stationarity of this functional corresponds to a saddle point problem. Therefore, the model derivation based on HR functional requires a particular care on the displacement and stress field assumptions, otherwise the model risks to lead to a problem lacking well-posedness.

3.2.1 HR grad-grad stationarity

Requiring stationarity of HR functional (4), we obtain the following weak problem: Find $\mathbf{s} \in W_{\bar{\mathbf{s}}}^{gg}$ and $\boldsymbol{\sigma} \in S^{gg}$ such that $\forall \delta \mathbf{s} \in \overline{W}^{gg}$ and $\forall \delta \boldsymbol{\sigma} \in S^{gg}$:

$$\delta J_{HR}^{gg} = \int_{\Omega} \nabla^s \delta \mathbf{s} : \boldsymbol{\sigma} \, d\Omega + \int_{\Omega} \delta \boldsymbol{\sigma} : \nabla^s \mathbf{s} \, d\Omega - \int_{\Omega} \delta \boldsymbol{\sigma} : \mathbf{D}^{-1} : \boldsymbol{\sigma} \, d\Omega - \int_{\Omega} \delta \mathbf{s} \cdot \mathbf{f} \, d\Omega - \int_{\partial\Omega_t} \delta \mathbf{s} \cdot \mathbf{t} \, dS = 0 \quad (5)$$

where

$$W_{\bar{\mathbf{s}}}^{gg} := \{\mathbf{s} \in H^1(\Omega) : \mathbf{s}|_{\partial\Omega_s} = \bar{\mathbf{s}}\}; \quad \overline{W}^{gg} := \{\delta \mathbf{s} \in H^1(\Omega) : \delta \mathbf{s}|_{\partial\Omega_s} = \mathbf{0}\}; \quad S^{gg} := \{\boldsymbol{\sigma} \in L^2(\Omega)\}$$

We call Equation (5) **HR grad-grad stationarity** because two gradient operators appear in the formulation. We remark that the kinematic boundary condition $\mathbf{s}|_{\partial\Omega_s} = \bar{\mathbf{s}}$ is directly enforced in the trial space $W_{\bar{\mathbf{s}}}^{gg}$ (*essential* boundary condition), while $\boldsymbol{\sigma} \cdot \mathbf{n}|_{\partial\Omega_t} = \mathbf{t}$ turns out to be a *natural* boundary condition.

As anticipated in Section 1, Alessandrini et al. (1999) derived some homogeneous plate models starting from HR grad-grad stationarity (5). They noticed that in many situations, models derived by HR grad-grad stationarity (5) lead to model displacement fields which minimize the potential energy in the class of the same kinematic assumptions. Therefore, in those cases HR grad-grad models are essentially equivalent to the corresponding models obtained by the TPE symmetric stationarity (3).

Many researchers have derived multilayered plate and beam FE using HR grad-grad stationarity (5). The works by Spilker (1982), Feng and Hoa (1998), Icardi and Atzori (2004) and Huang et al. (2002) are among the most significant examples, since the computed solutions are generally satisfactory. The main drawback of these schemes, especially for the case of layer-wise beams and plates, is the high number of degrees of freedom (DOFs) that leads to an heavy FE formulation. Spilker (1982) alleviates this problem by assuming stress variables to be discontinuous along the plate extension so that they can be condensed at the element level reducing the mixed local stiffness matrix to a displacement-like one. An alternative is to consider some stress components as dependent variables, expressing them *a-priori* in terms of the displacements. Reissner's Mixed Variational Theorem, introduced by Reissner (1986), follows this approach: the out of plane stresses τ_{xy} and σ_{yy} are considered as independent variables while the axial stress σ_{xx} is expressed as a function of displacements; Carrera (2000, 2001), Carrera and Demasi (2002) and Demasi (2009a,b,c,d,e) derived different plate FE applying this viewpoint, with different choice of basis function and obtaining a reasonable accuracy in stress description; unfortunately they are forced to use a high number of kinematic DOFs, drastically increasing the computational effort.

3.2.2 HR div-div stationarity

Integrating by parts, the first and the second terms of Equation (5) become:

$$\begin{aligned} \int_{\Omega} \nabla^s \delta \mathbf{s} : \boldsymbol{\sigma} \, d\Omega &= \int_{\partial\Omega} \delta \mathbf{s} \cdot \boldsymbol{\sigma} \cdot \mathbf{n} \, dS - \int_{\Omega} \delta \mathbf{s} \cdot \nabla \cdot \boldsymbol{\sigma} \, d\Omega \\ \int_{\Omega} \delta \boldsymbol{\sigma} : \nabla^s \mathbf{s} \, d\Omega &= \int_{\partial\Omega} \delta \boldsymbol{\sigma} \cdot \mathbf{n} \cdot \mathbf{s} \, dS - \int_{\Omega} \nabla \cdot \delta \boldsymbol{\sigma} \cdot \mathbf{s} \, d\Omega \end{aligned} \quad (6)$$

Hence, substituting Expression (6) in (5), the weak formulation becomes:

Find $\mathbf{s} \in W^{dd}$ and $\boldsymbol{\sigma} \in S_t^{dd}$ such that $\forall \delta \mathbf{s} \in W^{dd}$ and $\forall \delta \boldsymbol{\sigma} \in \overline{S}^{dd}$

$$\begin{aligned} \delta J_{HR}^{dd} = & - \int_{\Omega} \delta \mathbf{s} \cdot \nabla \cdot \boldsymbol{\sigma} \, d\Omega - \int_{\Omega} \nabla \cdot \delta \boldsymbol{\sigma} \cdot \mathbf{s} \, d\Omega - \int_{\Omega} \delta \boldsymbol{\sigma} : \mathbf{D}^{-1} : \boldsymbol{\sigma} \, d\Omega - \int_{\Omega} \delta \mathbf{s} \cdot \mathbf{f} \, d\Omega \\ & + \int_{\partial\Omega_s} \delta \boldsymbol{\sigma} \cdot \mathbf{n} \cdot \overline{\boldsymbol{\sigma}} \, dS = 0 \end{aligned} \quad (7)$$

where

$$W^{dd} := \{\mathbf{s} \in L^2(\Omega)\}$$

$$S_t^{dd} := \{\boldsymbol{\sigma} \in H(\text{div}, \Omega) : \boldsymbol{\sigma} \cdot \mathbf{n}|_{\partial\Omega_t} = \mathbf{t}\}; \quad \overline{S}^{dd} := \{\delta \boldsymbol{\sigma} \in H(\text{div}, \Omega) : \delta \boldsymbol{\sigma} \cdot \mathbf{n}|_{\partial\Omega_t} = \mathbf{0}\}$$

Here above and in what follows, $H(\text{div}, \Omega)$ denotes the space of vectorial square-integrable functions, whose divergence is still square-integrable. We define Equation (7) as **HR div-div stationarity** because two divergence operators appear in it. We remark that $\mathbf{s}|_{\partial\Omega_s} = \overline{\boldsymbol{\sigma}}$ is now a *natural* boundary condition, while $\boldsymbol{\sigma} \cdot \mathbf{n}|_{\partial\Omega_t} = \mathbf{t}$ becomes an *essential* boundary condition, as it is directly incorporated in the space S_t^{dd} .

Considering the HR div-div stationarity approach (7), Alessandrini et al. have derived some homogeneous plate models, more interesting than the ones stemming from the HR grad-grad stationarity (5). However, the same techniques developed in Alessandrini et al. cannot be directly applied to general heterogeneous plates, because the resulting models may be divergent (cf. Auricchio et al. (2004)).

3.3 Hu-Washizu approach

The Hu-Washizu (shortly HW) functional may be expressed as follows:

$$J_{HW}(\boldsymbol{\sigma}, \boldsymbol{\varepsilon}, \mathbf{s}) = \int_{\Omega} \boldsymbol{\sigma} : (\nabla^s \mathbf{s} - \boldsymbol{\varepsilon}) \, d\Omega + \frac{1}{2} \int_{\Omega} \boldsymbol{\varepsilon} : \mathbf{D} : \boldsymbol{\varepsilon} \, d\Omega - \int_{\Omega} \mathbf{s} \cdot \mathbf{f} \, d\Omega \quad (8)$$

Again, how boundary conditions will be enforced depends on the specific variational formulation employed to express the stationarity of the functional. We also remark that, here, also the strain field is a primal variable. In the following variational formulations, we will not specify the functional frameworks for the involved fields, since they are similar to the ones of the HR-based corresponding variational formulations.

3.3.1 HW grad-grad stationarity

Stationarity of Equation (8) can be expressed as:

$$\begin{aligned} \delta J_{HW}^{gg} = & \int_{\Omega} \nabla^s \delta \mathbf{s} : \boldsymbol{\sigma} \, d\Omega - \int_{\Omega} \delta \boldsymbol{\varepsilon} : \boldsymbol{\sigma} \, d\Omega + \int_{\Omega} \delta \boldsymbol{\sigma} : (\nabla^s \mathbf{s} - \boldsymbol{\varepsilon}) \, d\Omega + \int_{\Omega} \delta \boldsymbol{\varepsilon} : \mathbf{D} : \boldsymbol{\varepsilon} \, d\Omega \\ & - \int_{\Omega} \delta \mathbf{s} \cdot \mathbf{f} \, d\Omega - \int_{\partial\Omega_t} \delta \mathbf{s} \cdot \mathbf{t} \, dS = 0 \end{aligned} \quad (9)$$

where \mathbf{s} satisfies $\mathbf{s}|_{\partial\Omega_s} = \overline{\boldsymbol{\sigma}}$, while $\boldsymbol{\sigma} \cdot \mathbf{n}|_{\partial\Omega_t} = \mathbf{t}$ is a natural boundary condition. As in the discussion of HR stationarities we call Equation (9) **HW grad-grad stationarity** because two gradient operators appear in the formulation. An example of the use of HW grad-grad stationarity (9) in multilayered plate modeling is presented by Auricchio and Sacco (1999).

3.3.2 HW div-div stationarity

A second HW stationarity formulation can be found introducing Equations (6) in Equation (9) obtaining:

$$\begin{aligned} \delta J_{HW}^{dd} = & - \int_{\Omega} \delta \mathbf{s} \cdot \nabla \cdot \boldsymbol{\sigma} d\Omega - \int_{\Omega} \delta \boldsymbol{\varepsilon} : \boldsymbol{\sigma} d\Omega - \int_{\Omega} \nabla \cdot \delta \boldsymbol{\sigma} \cdot \mathbf{s} d\Omega - \int_{\Omega} \delta \boldsymbol{\sigma} : \boldsymbol{\varepsilon} d\Omega + \int_{\Omega} \delta \boldsymbol{\varepsilon} : \mathbf{D} : \boldsymbol{\varepsilon} d\Omega \\ & - \int_{\Omega} \delta \mathbf{s} \cdot \mathbf{f} d\Omega + \int_{\partial\Omega_s} (\delta \boldsymbol{\sigma} \cdot \mathbf{n}) \cdot \bar{\mathbf{s}} dS = 0 \end{aligned} \quad (10)$$

where $\boldsymbol{\sigma}$ satisfies $\boldsymbol{\sigma} \cdot \mathbf{n} = \mathbf{t}$ on $\partial\Omega_t$, while $\mathbf{s}|_{\partial\Omega_s} = \bar{\mathbf{s}}$ is a natural boundary condition. We call Equation (10) **HW div-div stationarity** because two divergence operators appear in the formulation.

3.4 Conclusions on problem weak formulations

From the previous discussion (briefly summarized in Table 1 in terms of principles and equation formats) it is possible to draw some concluding remarks, listed in the following.

- All the considered weak problem formulations are symmetric.
- Every mixed weak formulation can be expressed in different formats: the grad-grad formulations (5) and (9), and the div-div formulations (7) and (10). The former ones require to consider *a-priori* smooth displacement fields and less regular stress fields ($\mathbf{s} \in H^1(\Omega)$ and $\boldsymbol{\sigma} \in L^2(\Omega)$), while the latter ones demand *a-priori* less regular displacement fields and smooth stress fields ($\mathbf{s} \in L^2(\Omega)$ and $\boldsymbol{\sigma} \in H(\text{div}, \Omega)$).
- When selecting the approximation fields for the mixed model design (cf. **Second step** of the procedure described at the beginning of this Section), the combination of the regularity requirements and the well-posedness of the corresponding saddle point problems, typically leads to
 - congruent models for the grad-grad formulations
 - self-equilibrated models for the div-div formulations.

Since we think that one of the major limitations of the elementary available beam models is connected to the fact that equilibrium equations are not sufficiently enforced within the cross-section, in the following we focus on HR formulations but with some emphasis on the div-div form (7).

	Principle	
displacement-based	TPE	eq (3)
mixed	HR	grad-grad eq (5) div-div eq (7)
	HW	grad-grad eq (9) div-div eq (10)

Table 1: Obtained functional stationarities classified in terms of functionals from which are derived and equation formats.

4 Model derivations

In this section we develop some beam models. Referring to the procedure described at the beginning of Section 3, we will start from the HR variational formulations of Section 3.2 (cf. **First step**), we will define the approximated fields (cf. **Second step**), and perform the integration along the thickness (cf. **Third step**). Moreover, to simplify the further discussions, we will switch to an engineering notation.

4.1 Profile approximation and notations

We now introduce the notation we use for a generic approximated field $\gamma(x, y)$ involved in the beam models. We first define a *profile* vectorial function $\mathbf{p}_\gamma(y)$:

$$\mathbf{p}_\gamma : A \rightarrow \mathbb{R}^m$$

We insist that the m components of $\mathbf{p}_\gamma(y)$ are a set of *linearly independent* functions of the cross-section coordinate y . They may be global polynomials, as well as piece-wise polynomials or other shape functions. The approximate field $\gamma(x, y)$ is expressed as a linear combination of the components of $\mathbf{p}_\gamma(y)$, with arbitrary functions of the axial coordinate x as coefficients, collected in a vector $\hat{\gamma}(x)$. Therefore, $\gamma(x, y)$ can be written as a scalar product between $\mathbf{p}_\gamma(y)$ and $\hat{\gamma}(x)$, i.e.

$$\gamma(x, y) = \mathbf{p}_\gamma^T(y) \hat{\gamma}(x) \quad (11)$$

where the superscript T denotes the transposition operation, and

$$\hat{\gamma} : l \rightarrow \mathbb{R}^m$$

contains the functional coefficients as components. We emphasize that, once the profile vector $\mathbf{p}_\gamma(y)$ has been assigned, the field $\gamma(x, y)$ is uniquely determined by the components of $\hat{\gamma}(x)$. Such components, for all the involved fields, are indeed the *unknowns* of the beam models we will develop. We also remark that, due to assumption (11), computation of partial derivatives is straightforward, since it holds:

$$\frac{\partial}{\partial x} \gamma = \frac{\partial}{\partial x} (\mathbf{p}_\gamma^T \hat{\gamma}) = \mathbf{p}_\gamma^T \frac{d}{dx} \hat{\gamma} = \mathbf{p}_\gamma^T \hat{\gamma}' \quad \frac{\partial}{\partial y} \gamma = \frac{\partial}{\partial y} (\mathbf{p}_\gamma^T \hat{\gamma}) = \frac{d}{dy} \mathbf{p}_\gamma^T \hat{\gamma} = \mathbf{p}_\gamma'^T \hat{\gamma}$$

where we use a prime to indicate derivatives both along x and along y , because there is no risk of confusion. Adopting notation introduced in (11) and switching now to an engineering notation we set:

$$\mathbf{s}(x, y) = \begin{Bmatrix} s_u(x, y) \\ s_v(x, y) \end{Bmatrix} = \begin{bmatrix} \mathbf{p}_u^T(y) & \mathbf{0} \\ \mathbf{0} & \mathbf{p}_v^T(y) \end{bmatrix} \begin{Bmatrix} \hat{\mathbf{u}}(x) \\ \hat{\mathbf{v}}(x) \end{Bmatrix} = \mathbf{P}_s \hat{\mathbf{s}} \quad (12)$$

$$\boldsymbol{\sigma}(x, y) = \begin{Bmatrix} \sigma_{xx}(x, y) \\ \sigma_{yy}(x, y) \\ \tau_{xy}(x, y) \end{Bmatrix} = \begin{bmatrix} \mathbf{p}_{\sigma_x}^T(y) & \mathbf{0} & \mathbf{0} \\ \mathbf{0} & \mathbf{p}_{\sigma_y}^T(y) & \mathbf{0} \\ \mathbf{0} & \mathbf{0} & \mathbf{p}_\tau^T(y) \end{bmatrix} \begin{Bmatrix} \hat{\sigma}_x(x) \\ \hat{\sigma}_y(x) \\ \hat{\tau}(x) \end{Bmatrix} = \mathbf{P}_\sigma \hat{\boldsymbol{\sigma}} \quad (13)$$

where, for \mathbf{P}_s and \mathbf{P}_σ ($\hat{\mathbf{s}}$ and $\hat{\boldsymbol{\sigma}}$, respectively), we drop the explicit dependence on y (x , respectively), for notational simplicity. Virtual fields are analogously defined as:

$$\delta \mathbf{s} = \mathbf{P}_s \delta \hat{\mathbf{s}} \quad \delta \boldsymbol{\sigma} = \mathbf{P}_\sigma \delta \hat{\boldsymbol{\sigma}}$$

Coherently with the engineering notation just introduced, in Table 2 we re-define the differential operators and the normal vector product where

$$\mathbf{E}_1 = \begin{bmatrix} 1 & 0 & 0 \\ 0 & 0 & 1 \end{bmatrix} \quad \mathbf{E}_2 = \begin{bmatrix} 0 & 0 & 1 \\ 0 & 1 & 0 \end{bmatrix}$$

In Section 3, with \mathbf{D}^{-1} we denoted the fourth order elastic tensor while from now on, we use the same notation to indicate the corresponding square matrix obtained following engineering notation. Therefore, we have:

$$\mathbf{D}^{-1} = \frac{1}{E} \begin{bmatrix} 1 & -\nu & 0 \\ -\nu & 1 & 0 \\ 0 & 0 & 2(1+\nu) \end{bmatrix}$$

Tensorial notation	Engineering notation
$\nabla \cdot \boldsymbol{\sigma}$	$\left(\frac{d}{dx} \mathbf{E}_1 + \frac{d}{dy} \mathbf{E}_2 \right) \mathbf{P}_\sigma \hat{\boldsymbol{\sigma}}$
$\nabla^S \mathbf{s}$	$\left(\frac{d}{dx} \mathbf{E}_1^T + \frac{d}{dy} \mathbf{E}_2^T \right) \mathbf{P}_s \hat{\mathbf{s}}$
$\boldsymbol{\sigma} \cdot \mathbf{n}$	$(n_x \mathbf{E}_1 + n_y \mathbf{E}_2) \mathbf{P}_\sigma \hat{\boldsymbol{\sigma}}$

Table 2: Tensorial and Engineering equivalent notations.

4.2 Problem formulations

In the following, we consider the special case of a beam for which it holds:

$$\begin{aligned} \bar{\mathbf{s}} &= \mathbf{0} & \text{on } A_0 = \partial\Omega_s, & & \mathbf{t} &\neq \mathbf{0} & \text{on } A_l \\ \mathbf{f} &= \mathbf{0} & \text{in } \Omega, & & \mathbf{t} &= \mathbf{0} & \text{on } S_0 \cup S_n \end{aligned}$$

Hence, $\partial\Omega_t = A_l \cup S_0 \cup S_n$; moreover, the beam is clamped on the left-hand side A_0 , and it is subjected to a non-vanishing traction field on the right-hand side A_l . Furthermore, we suppose that $\mathbf{t}|_{A_l}$ can be exactly represented using the chosen profiles for $\boldsymbol{\sigma} \cdot \mathbf{n}$. Recalling (13), and noting that $\mathbf{n}|_{A_l} = (1, 0)^T$, this means that there exist suitable vectors $\hat{\mathbf{t}}_x$ and $\hat{\mathbf{t}}_\tau$ such that

$$\mathbf{t} = \begin{Bmatrix} \mathbf{P}_{\sigma_x}^T \hat{\mathbf{t}}_x \\ \mathbf{P}_\tau^T \hat{\mathbf{t}}_\tau \end{Bmatrix} \quad (14)$$

Therefore, the boundary condition $\boldsymbol{\sigma} \cdot \mathbf{n}|_{A_l} = \mathbf{t}$ may be written as (cf. (13))

$$\begin{Bmatrix} \hat{\boldsymbol{\sigma}}_x(\bar{l}) \\ \hat{\boldsymbol{\tau}}(\bar{l}) \end{Bmatrix} = \begin{Bmatrix} \hat{\mathbf{t}}_x \\ \hat{\mathbf{t}}_\tau \end{Bmatrix} \quad (15)$$

We also remark that all these assumptions can be modified to cover more general cases; nonetheless, this simple model is already adequate to illustrate the method capabilities.

4.2.1 HR grad-grad approach

Using the notations introduced in Subsection 4.1 the HR grad-grad stationarity (5) becomes:

$$\begin{aligned} \delta J_{HR}^{gg} &= \int_{\Omega} \left[\left(\frac{d}{dx} \mathbf{E}_1^T + \frac{d}{dy} \mathbf{E}_2^T \right) \mathbf{P}_s \delta \hat{\mathbf{s}} \right]^T \mathbf{P}_\sigma \hat{\boldsymbol{\sigma}} d\Omega + \int_{\Omega} \delta \hat{\boldsymbol{\sigma}}^T \mathbf{P}_\sigma^T \left[\left(\frac{d}{dx} \mathbf{E}_1^T + \frac{d}{dy} \mathbf{E}_2^T \right) \mathbf{P}_s \hat{\mathbf{s}} \right] d\Omega \\ &\quad - \int_{\Omega} \delta \hat{\boldsymbol{\sigma}}^T \mathbf{P}_\sigma^T \mathbf{D}^{-1} \mathbf{P}_\sigma \hat{\boldsymbol{\sigma}} d\Omega - \int_{\partial\Omega_t} \delta \hat{\mathbf{s}}^T \mathbf{P}_s^T \mathbf{t} dy = 0 \end{aligned} \quad (16)$$

Expanding Equation (16) we obtain:

$$\begin{aligned} \delta J_{HR}^{gg} &= \int_{\Omega} \left(\delta \hat{\mathbf{s}}'^T \mathbf{P}_s^T \mathbf{E}_1 \mathbf{P}_\sigma \hat{\boldsymbol{\sigma}} + \delta \hat{\mathbf{s}}^T \mathbf{P}_s'^T \mathbf{E}_2 \mathbf{P}_\sigma \hat{\boldsymbol{\sigma}} \right) d\Omega + \int_{\Omega} \left(\delta \hat{\boldsymbol{\sigma}}^T \mathbf{P}_\sigma^T \mathbf{E}_1^T \mathbf{P}_s \hat{\mathbf{s}}' + \delta \hat{\boldsymbol{\sigma}}^T \mathbf{P}_\sigma^T \mathbf{E}_2^T \mathbf{P}_s' \hat{\mathbf{s}} \right) d\Omega \\ &\quad - \int_{\Omega} \delta \hat{\boldsymbol{\sigma}}^T \mathbf{P}_\sigma^T \mathbf{D}^{-1} \mathbf{P}_\sigma \hat{\boldsymbol{\sigma}} d\Omega - \int_{A_l} \delta \hat{\mathbf{s}}^T \mathbf{P}_s^T \mathbf{t} dy = 0 \end{aligned} \quad (17)$$

By using Fubini-Tonelli theorem, Equation (17) can be written as:

$$\delta J_{HR}^{gg} = \int_l \left(\delta \hat{\mathbf{s}}'^T \mathbf{G}_{s\sigma} \hat{\boldsymbol{\sigma}} + \delta \hat{\mathbf{s}}^T \mathbf{H}_{s'\sigma} \hat{\boldsymbol{\sigma}} + \delta \hat{\boldsymbol{\sigma}}^T \mathbf{G}_{\sigma s} \hat{\mathbf{s}}' + \delta \hat{\boldsymbol{\sigma}}^T \mathbf{H}_{\sigma s'} \hat{\mathbf{s}} - \delta \hat{\boldsymbol{\sigma}}^T \mathbf{H}_{\sigma\sigma} \hat{\boldsymbol{\sigma}} \right) dx - \delta \hat{\mathbf{s}}^T \mathbf{T}_x \Big|_{x=\bar{l}} = 0 \quad (18)$$

where:

$$\begin{aligned} \mathbf{G}_{s\sigma} &= \mathbf{G}_{\sigma s}^T = \int_A \mathbf{P}_s^T \mathbf{E}_1 \mathbf{P}_\sigma dy & \mathbf{H}_{\sigma\sigma} &= \int_A \mathbf{P}_\sigma^T \mathbf{D}^{-1} \mathbf{P}_\sigma dy \\ \mathbf{H}_{s'\sigma} &= \mathbf{H}_{\sigma s'}^T = \int_A \mathbf{P}'_s{}^T \mathbf{E}_2 \mathbf{P}_\sigma dy & \mathbf{T}_x &= \int_{A_l} \mathbf{P}'_s{}^T \mathbf{t} dy \end{aligned} \quad (19)$$

Equation (18) represents the weak form of the 1D beam model. To obtain the corresponding boundary value problem, we integrate by parts the first term of (18):

$$\int_l \delta \hat{\mathbf{s}}'^T \mathbf{G}_{s\sigma} \hat{\boldsymbol{\sigma}} dx = \delta \hat{\mathbf{s}}^T \mathbf{G}_{s\sigma} \hat{\boldsymbol{\sigma}} \Big|_{x=0}^{x=\bar{l}} - \int_l \delta \hat{\mathbf{s}}^T \mathbf{G}_{s\sigma} \hat{\boldsymbol{\sigma}}' dx \quad (20)$$

Substituting Equation (20) in (18), recalling that $\delta \hat{\mathbf{s}} = \mathbf{0}$ on A_0 and collecting variables in a vector we obtain:

$$\int_l [\delta \hat{\mathbf{s}}; \delta \hat{\boldsymbol{\sigma}}]^T \left(\mathbf{G} \begin{Bmatrix} \hat{\mathbf{s}}' \\ \hat{\boldsymbol{\sigma}}' \end{Bmatrix} + \mathbf{H}^{gg} \begin{Bmatrix} \hat{\mathbf{s}} \\ \hat{\boldsymbol{\sigma}} \end{Bmatrix} \right) dx + \delta \hat{\mathbf{s}}^T (\mathbf{G}_{s\sigma} \hat{\boldsymbol{\sigma}} - \mathbf{T}_x) \Big|_{x=\bar{l}} = 0 \quad (21)$$

in which

$$\mathbf{G} = \begin{bmatrix} \mathbf{0} & -\mathbf{G}_{s\sigma} \\ \mathbf{G}_{\sigma s} & \mathbf{0} \end{bmatrix} \quad \mathbf{H}^{gg} = \begin{bmatrix} \mathbf{0} & \mathbf{H}_{s'\sigma} \\ \mathbf{H}_{\sigma s'} & -\mathbf{H}_{\sigma\sigma} \end{bmatrix} \quad (22)$$

Requiring to satisfy Equation (21) for all the possible variations, and imposing the *essential* boundary condition $\hat{\mathbf{s}}$ we finally obtain:

$$\begin{cases} \mathbf{G} \begin{Bmatrix} \hat{\mathbf{s}}' \\ \hat{\boldsymbol{\sigma}}' \end{Bmatrix} + \mathbf{H}^{gg} \begin{Bmatrix} \hat{\mathbf{s}} \\ \hat{\boldsymbol{\sigma}} \end{Bmatrix} = \begin{Bmatrix} \mathbf{0} \\ \mathbf{0} \end{Bmatrix} & \text{in } l \\ \mathbf{G}_{s\sigma} \hat{\boldsymbol{\sigma}} = \mathbf{T}_x & \text{at } x = \bar{l} \\ \hat{\mathbf{s}} = \mathbf{0} & \text{at } x = 0 \end{cases} \quad (23)$$

We remark that boundary value problem (23) is not necessarily well-posed. This depends on how the profile vectors have been chosen for all the involved fields. However, well-posedness of (23) is guaranteed if the approximated fields are selected according with the approximation theory of saddle-point problem (5) (see Alessandrini et al. (1999)).

4.2.2 HR div-div approach

Using the notation introduced in Section 4.1 in Equation (7), the HR div-div functional stationarity becomes:

$$\begin{aligned} \delta J_{HR}^{dd} &= - \int_\Omega \delta \hat{\mathbf{s}}^T \mathbf{P}_s^T \left[\left(\frac{d}{dx} \mathbf{E}_1 + \frac{d}{dy} \mathbf{E}_2 \right) \mathbf{P}_\sigma \hat{\boldsymbol{\sigma}} \right] d\Omega - \int_\Omega \left[\left(\frac{d}{dx} \mathbf{E}_1 + \frac{d}{dy} \mathbf{E}_2 \right) \mathbf{P}_\sigma \delta \hat{\boldsymbol{\sigma}} \right]^T \mathbf{P}_s \hat{\mathbf{s}} d\Omega \\ &\quad - \int_\Omega \delta \hat{\boldsymbol{\sigma}}^T \mathbf{P}_\sigma^T \mathbf{D}^{-1} \mathbf{P}_\sigma \hat{\boldsymbol{\sigma}} d\Omega = 0 \end{aligned} \quad (24)$$

Expanding Equation (24), the weak formulation becomes:

$$\begin{aligned} \delta J_{HR}^{dd} &= - \int_\Omega \left(\delta \hat{\mathbf{s}}^T \mathbf{P}_s^T \mathbf{E}_1 \mathbf{P}_\sigma \hat{\boldsymbol{\sigma}}' + \delta \hat{\mathbf{s}}^T \mathbf{P}_s^T \mathbf{E}_2 \mathbf{P}'_\sigma \hat{\boldsymbol{\sigma}} \right) d\Omega - \int_\Omega \left(\delta \hat{\boldsymbol{\sigma}}'^T \mathbf{P}_\sigma^T \mathbf{E}_1^T \mathbf{P}_s \hat{\mathbf{s}} + \delta \hat{\boldsymbol{\sigma}}^T \mathbf{P}'_\sigma{}^T \mathbf{E}_2^T \mathbf{P}_s \hat{\mathbf{s}} \right) d\Omega \\ &\quad - \int_\Omega \delta \hat{\boldsymbol{\sigma}}^T \mathbf{P}_\sigma^T \mathbf{D}^{-1} \mathbf{P}_\sigma \hat{\boldsymbol{\sigma}} d\Omega = 0 \end{aligned} \quad (25)$$

By using Fubini-Tonelli theorem, Equation (25) becomes:

$$\delta J_{HR}^{dd} = \int_l \left(-\delta \hat{\mathbf{s}}^T \mathbf{G}_{s\sigma} \hat{\boldsymbol{\sigma}}' - \delta \hat{\mathbf{s}}^T \mathbf{H}_{s'\sigma} \hat{\boldsymbol{\sigma}} - \delta \hat{\boldsymbol{\sigma}}'^T \mathbf{G}_{\sigma s} \hat{\mathbf{s}} - \delta \hat{\boldsymbol{\sigma}}^T \mathbf{H}_{\sigma s'} \hat{\mathbf{s}} - \delta \hat{\boldsymbol{\sigma}}^T \mathbf{H}_{\sigma\sigma} \hat{\boldsymbol{\sigma}} \right) dx = 0 \quad (26)$$

where

$$\mathbf{H}_{\sigma's} = \int_A \mathbf{P}'^T \mathbf{E}_2 \mathbf{P}_s dy$$

while the other matrices are defined as (19).

Equation (26) represents the weak form of the 1D beam model. To obtain the corresponding boundary value problem, we integrate by parts the third term of (26):

$$- \int_l \delta \hat{\boldsymbol{\sigma}}'^T \mathbf{G}_{\sigma s} \hat{\boldsymbol{\sigma}} dx = - \delta \hat{\boldsymbol{\sigma}}'^T \mathbf{G}_{\sigma s} \hat{\boldsymbol{\sigma}} \Big|_{x=0}^{x=\bar{l}} + \int_l \delta \hat{\boldsymbol{\sigma}}'^T \mathbf{G}_{\sigma s} \hat{\boldsymbol{\sigma}}' dx \quad (27)$$

Substituting Equation (27) in Equation (26), recalling that $\mathbf{G}_{s\sigma} \delta \hat{\boldsymbol{\sigma}} = \mathbf{0}$ at $x = \bar{l}$, and collecting the unknowns in a vector we obtain:

$$\int_l [\delta \hat{\boldsymbol{\sigma}}; \delta \hat{\boldsymbol{\sigma}}']^T \left(\mathbf{G} \begin{Bmatrix} \hat{\boldsymbol{\sigma}}' \\ \hat{\boldsymbol{\sigma}} \end{Bmatrix} + \mathbf{H}^{dd} \begin{Bmatrix} \hat{\boldsymbol{\sigma}} \\ \hat{\boldsymbol{\sigma}}' \end{Bmatrix} \right) dx + \delta \hat{\boldsymbol{\sigma}}'^T \mathbf{G}_{\sigma s} \hat{\boldsymbol{\sigma}} \Big|_{x=0} = 0 \quad (28)$$

where \mathbf{G} is defined as in (22) and \mathbf{H}^{dd} is defined as:

$$\mathbf{H}^{dd} = \begin{bmatrix} \mathbf{0} & -\mathbf{H}_{s\sigma'} \\ -\mathbf{H}_{\sigma's} & -\mathbf{H}_{\sigma\sigma} \end{bmatrix} \quad (29)$$

Requiring to satisfy Equation (28) for all the possible variations, and imposing the *essential* boundary condition (15), we finally obtain:

$$\begin{cases} \mathbf{G} \begin{Bmatrix} \hat{\boldsymbol{\sigma}}' \\ \hat{\boldsymbol{\sigma}} \end{Bmatrix} + \mathbf{H}^{dd} \begin{Bmatrix} \hat{\boldsymbol{\sigma}} \\ \hat{\boldsymbol{\sigma}}' \end{Bmatrix} = \begin{Bmatrix} \mathbf{0} \\ \mathbf{0} \end{Bmatrix} & \text{in } l \\ \hat{\boldsymbol{\sigma}}_x = \hat{\mathbf{t}}_x & \text{at } x = \bar{l} \\ \hat{\boldsymbol{\tau}} = \hat{\mathbf{t}}_\tau & \text{at } x = \bar{l} \\ \mathbf{G}_{\sigma s} \hat{\boldsymbol{\sigma}} = \mathbf{0} & \text{at } x = 0 \end{cases} \quad (30)$$

We remark that boundary value problem (30) is not necessarily well-posed. This depends on how the profile vectors have been chosen for all the involved fields. However, well-posedness of (30) is guaranteed if the approximated fields are selected according with the approximation theory of saddle-point problem (7) (see Alessandrini et al. (1999)).

4.3 Conclusions on the derived beam models

From what we have developed in this section, we can make the following remarks.

- Starting from two different versions of the HR stationarity condition (i.e., grad-grad (5) and div-div (7)) and introducing hypothesis (11), we obtain two different classes of one-dimensional beam models. Both classes may be described by a boundary value problem of the following type:

$$\begin{cases} \mathbf{G} \begin{Bmatrix} \hat{\boldsymbol{\sigma}}' \\ \hat{\boldsymbol{\sigma}} \end{Bmatrix} + \mathbf{H} \begin{Bmatrix} \hat{\boldsymbol{\sigma}} \\ \hat{\boldsymbol{\sigma}}' \end{Bmatrix} = \begin{Bmatrix} \mathbf{0} \\ \mathbf{0} \end{Bmatrix} \\ + \text{suitable boundary conditions} \end{cases} \quad (31)$$

The difference between models based on the HR grad-grad formulation and the HR div-div one stands in the \mathbf{H} matrix. More precisely:

- $\mathbf{H} = \mathbf{H}^{gg}$ for the HR grad-grad formulation. In this case, derivatives are applied to the displacement fields through the symmetric gradient operator, and most likely the resulting models strongly satisfy the compatibility law, but not necessarily the equilibrium equation.

- $\mathbf{H} = \mathbf{H}^{dd}$ for the HR div-div formulation. In this case, derivatives are applied to the stress fields through the divergence operator, and most likely the resulting models strongly satisfy the equilibrium equation, but not the necessarily the compatibility one.

- Boundary value problem (30) can be explicitly written as:

$$\begin{cases} -\mathbf{G}_{s\sigma}\hat{\boldsymbol{\sigma}}' - \mathbf{H}_{s\sigma'}\hat{\boldsymbol{\sigma}} = \mathbf{0} \\ \mathbf{G}_{\sigma s}\hat{\boldsymbol{s}}' - \mathbf{H}_{\sigma's}\hat{\boldsymbol{s}} - \mathbf{H}_{\sigma\sigma}\hat{\boldsymbol{\sigma}} = \mathbf{0} \\ + \text{suitable boundary conditions} \end{cases}$$

We can compute $\hat{\boldsymbol{\sigma}}$ from the second equation and substitute it in the first one, obtaining a displacement-like formulation of the problem:

$$\begin{cases} \mathbf{A}\hat{\boldsymbol{s}}'' + \mathbf{B}\hat{\boldsymbol{s}}' + \mathbf{C}\hat{\boldsymbol{s}} = \begin{Bmatrix} \mathbf{0} \\ \mathbf{0} \end{Bmatrix} \\ + \text{suitable boundary conditions} \end{cases} \quad (32)$$

where

$$\mathbf{A} = -\mathbf{G}_{s\sigma}\mathbf{H}_{\sigma\sigma}^{-1}\mathbf{G}_{\sigma s} \quad \mathbf{B} = -\mathbf{G}_{s\sigma}\mathbf{H}_{\sigma\sigma}^{-1}\mathbf{H}_{\sigma's} + \mathbf{H}_{s\sigma'}\mathbf{H}_{\sigma\sigma}^{-1}\mathbf{G}_{\sigma s} \quad \mathbf{C} = \mathbf{H}_{s\sigma'}\mathbf{H}_{\sigma\sigma}^{-1}\mathbf{H}_{\sigma's}$$

Analogous considerations apply to problem (23).

5 Examples of beam models

In this section we give two examples of beam models developed using the strategies of Section 4. More precisely, starting from the HR div-div approach (Equation (30)), we derive:

1. a single layer beam model in which we use a first order displacement field; by means of this example we will show that the approach under discussion is able to reproduce the classical models;
2. a multilayer beam model, in which we consider also higher order kinematic and stress fields; by means of this example we will illustrate how the approach could produce a refined model with a reasonable solution.

5.1 Single layer beam

Considering a homogeneous beam, we assume a first-order kinematic (as in Timoshenko model) and the usual cross-section stress distributions (obtained from the Jourawsky theory). In other words we make the following hypotheses:

$$\begin{array}{llll} u = u_0(x) + yu_1(x) & \text{i.e.} & \mathbf{p}_u = \begin{Bmatrix} 1 \\ y \end{Bmatrix} & \hat{\mathbf{u}} = \begin{Bmatrix} u_0 \\ u_1 \end{Bmatrix} \\ v = v(x) & \text{i.e.} & \mathbf{p}_v = \{1\} & \hat{\mathbf{v}} = \{v\} \\ \sigma_{xx} = \sigma_{x0}(x) + y\sigma_{x1}(x) & \text{i.e.} & \mathbf{p}_{\sigma_x} = \begin{Bmatrix} 1 \\ y \end{Bmatrix} & \hat{\boldsymbol{\sigma}}_x = \begin{Bmatrix} \sigma_{x0} \\ \sigma_{x1} \end{Bmatrix} \\ \sigma_{yy} = 0 & \text{i.e.} & \mathbf{p}_{\sigma_y} = \{0\} & \hat{\boldsymbol{\sigma}}_y = \{0\} \\ \tau = (1 - 4y^2/h^2)\tau(x) & \text{i.e.} & \mathbf{p}_\tau = \{1 - 4y^2/h^2\} & \hat{\boldsymbol{\tau}} = \{\tau\} \end{array}$$

The matrices \mathbf{G} and \mathbf{H}^{dd} defined in (22) and (29), and entering into the beam model (30), are explicitly given by:

$$\mathbf{G} = \begin{bmatrix} 0 & 0 & 0 & -h & 0 & 0 \\ 0 & 0 & 0 & 0 & -\frac{h^3}{12} & 0 \\ 0 & 0 & 0 & 0 & 0 & -\frac{2}{3}h \\ h & 0 & 0 & 0 & 0 & 0 \\ 0 & \frac{h^3}{12} & 0 & 0 & 0 & 0 \\ 0 & 0 & \frac{2}{3}h & 0 & 0 & 0 \end{bmatrix}; \mathbf{H}^{dd} = \begin{bmatrix} 0 & 0 & 0 & 0 & 0 & 0 \\ 0 & 0 & 0 & 0 & 0 & \frac{2}{3}h \\ 0 & 0 & 0 & 0 & 0 & 0 \\ 0 & 0 & 0 & -\frac{h}{E} & 0 & 0 \\ 0 & 0 & 0 & 0 & -\frac{h^3}{12} \frac{1}{E} & 0 \\ 0 & \frac{2}{3}h & 0 & 0 & 0 & -\frac{8}{15}h \frac{2(1+\nu)}{E} \end{bmatrix} \quad (33)$$

Since problem (30) is governed by an ODE system with constant coefficients, the homogeneous solution can be analytically computed. For example, choosing

$$h = 1 \text{ [mm]} \quad l = 10 \text{ [mm]} \quad E = 10^5 \text{ [MPa]} \quad \nu = 0.25 \text{ [-]}$$

the homogeneous solution is given by

$$\begin{aligned} u_0 &= 5.00 \cdot 10^{-6} C_4 x + C_1 \\ u_1 &= 4.00 \cdot 10^{-6} C_6 x^2 + 5.00 \cdot 10^{-6} C_5 x + C_2 \\ v &= -(1.33 \cdot 10^{-5} C_6 x^3 + 5.00 \cdot 10^{-6} C_5 x^2 + 5.00 \cdot 10^{-1} C_2 x + C_3) + 10^{-5} C_6 x \\ \sigma_{x0} &= C_4 \\ \sigma_{x1} &= 4.00 C_6 x + C_5 \\ \tau &= C_6 \end{aligned} \quad (34)$$

in which C_i are arbitrary constants. The six constants of (34) may be determined by imposing the boundary conditions specified in (30). Indeed, for the beam model under consideration, the boundary conditions in (30) lead to a set of six linearly independent equations, since the matrix \mathbf{G}_{σ_s} (cf. (19) and (22)) is invertible.

We remark that the solution (34) is compatible with the one obtained by the Timoshenko beam model. However, we underline that the stress distributions along the beam axis are obtained directly from the model solution, and not by means of the displacement derivatives, as happens in classical formulations.

We also notice that, reducing the model to the displacement formulation (cf. (32)), we obtain the following ODE system:

$$\begin{cases} hEu_0'' = 0 \\ \frac{h^3}{12}Eu_1'' - \frac{5}{62} \frac{Eh}{(1+\nu)}(v' + u_1) = 0 \\ \frac{5}{62} \frac{Eh}{(1+\nu)}(v'' + u_1') = 0 \\ + \text{suitable boundary conditions} \end{cases} \quad (35)$$

Therefore, not surprisingly, we again recover the classical Timoshenko equations, where, however, the exact shear correction factor (5/6) automatically appears. The same result holds true in the framework of variational plate modelling proposed by Alessandrini et al. (1999).

5.2 Multilayered beam

We now consider a beam composed by n layers, as illustrated in Figure 2. The geometric and material parameters for the generic i -th layer are defined by the thickness h_i , the Young's modulus E_i and the Poisson ratio ν_i , collected in the n -dimensional vectors \mathbf{h} , \mathbf{E} and $\boldsymbol{\nu}$, respectively.

To design a multilayered beam model, we follow the two-step procedure described below.

1. In each layer, we choose suitable profiles for every field involved in the modeling. Of course, given a generic field, the simplest choice, which is the one we use in this paper, is to use the same profiles for every layer.
2. Across each interlayer, we impose the necessary continuity to ensure that the stresses belong to $H(\text{div})$.

As a consequence, given a generic field γ , it is possible to define its profile vector \mathbf{p}_γ , which is characterized by:

- The highest polynomial degree, with respect to y , used in a generic layer. This number is denoted by $\text{deg}(\mathbf{p}_\gamma)$ in what follows.
- The regularity across each interlayer: in the following, C^{-1} stands for no continuity requirement, C^0 for standard continuity requirement.

Since a main aim of this paper is to develop a model with an accurate stress description, a natural choice is to assume $\text{deg}(\mathbf{p}_\tau) = 2$, as in Jourawsky theory. To ensure well-posedness of the resulting model, we thus select the involved fields according to Table 3, where we also show the number of layer and global DOFs. Furthermore, we notice that we have to impose $\sigma_y = \tau = 0$ at the top and bottom of the beam.

	$\text{deg}(\mathbf{p}_\gamma)$	inter-layer continuity	layer DOF	global DOF
\mathbf{p}_u	1	C^{-1}	2	2n
\mathbf{p}_v	2	C^{-1}	3	3n
\mathbf{p}_{σ_x}	1	C^{-1}	2	2n
\mathbf{p}_{σ_y}	3	C^0	4	3n-1
\mathbf{p}_τ	2	C^0	3	2n-1

Table 3: Polynomial degrees of the profiles vectors, continuity properties and number of DOFs for a multilayered beam.

Remark 5.1. *More generally, to design a well-posed beam model one could choose*

$$\begin{aligned} \text{deg}(\mathbf{p}_{\sigma_x}) &= \text{deg}(\mathbf{p}_u) = \text{deg}(\mathbf{p}_\tau) - 1 \\ \text{deg}(\mathbf{p}_\tau) &= \text{deg}(\mathbf{p}_v) = \text{deg}(\mathbf{p}_{\sigma_y}) - 1 \end{aligned} \quad (36)$$

together with the $H(\text{div})$ regularity for the stress field.

5.2.1 A test case

We now present an easy case to test the model robustness. More precisely, we consider a *homogeneous* beam, but we treat it as if it were formed by three layers. Thus, the geometric and material properties are described by:

$$\mathbf{h} = \begin{Bmatrix} 0.300 \\ 0.367 \\ 0.333 \end{Bmatrix} [\text{mm}] \quad \mathbf{E} = \begin{Bmatrix} 10^5 \\ 10^5 \\ 10^5 \end{Bmatrix} [\text{MPa}] \quad \boldsymbol{\nu} = \begin{Bmatrix} 0.25 \\ 0.25 \\ 0.25 \end{Bmatrix} [-]$$

As a consequence, the total number of cross-section variables is 34. We notice that the boundary value problem (30) is uniquely solvable also in this case. However, we now have $\text{rank}(\mathbf{G}) = 22$, which means that problem (30) is actually a differential-algebraic boundary value problem. Thus, 22 variables are solutions of a differential problem, while the remaining 12 unknowns are algebraically determined by the former ones. We also remark that the boundary conditions in (30) actually lead to 22 independent constraints, since $\text{rank}(\mathbf{G}_{\sigma_s}) = 11$.

We now give the solution of the generalized eigenvalue problem $\det(\lambda \mathbf{G} + \mathbf{H}^{dd}) = 0$, which enters in the construction of the homogeneous solution of (30).

$$\lambda = \left\{ \begin{array}{l} 0 \\ \sim 0 \\ 11.430 \pm 3.870i \\ -11.430 \pm 3.870i \\ 7.481 \pm 2.585i \\ -7.481 \pm 2.585i \\ 4.023 \pm 2.520i \\ -4.023 \pm 2.520i \\ 15.520 \pm 6.021i \\ -15.520 \pm 6.021i \end{array} \right\} \begin{array}{l} [12] \\ [6] \\ [1] \\ [1] \\ [1] \\ [1] \\ [1] \\ [1] \\ [1] \\ [1] \end{array}$$

where in square brackets we show the eigenvalue multiplicities, and we used the symbol ~ 0 to denote eigenvalues which vanish up to the machine precision.

It is possible to evaluate also the homogeneous solution but, given the problem complexity, it is huge and we will not report it. Nevertheless it is possible to discuss its structure and made some important remarks.

- The zero eigenvalues lead to polynomial terms analogous to the Timoshenko homogeneous solution described in Section 5.1.
- The complex conjugate eigenvalues ($a \pm ib$) lead to functions like $C_i e^{ax} \sin(bx + C_j)$, which describe local effects near the boundaries, as it happens in several other beam models (see Ladeveze and Simmonds, 1998; Allix and Duplex-Couderc, 2009).

6 Numerical multilayered beam model

In this section we develop the FE corresponding to the multilayered beam model introduced in Section 5.2. This is equivalent to introduce a dimension reduction also along the beam axis, leading, therefore, to a purely algebraic system. The discretization of axial fields $\hat{\mathbf{s}}$ and $\hat{\boldsymbol{\sigma}}$ can be generally described as follows:

$$\begin{aligned} \hat{\mathbf{s}}(x) &\cong \mathbf{N}_s \tilde{\mathbf{s}} = \begin{bmatrix} \mathbf{N}_u(x) & \mathbf{0} \\ \mathbf{0} & \mathbf{N}_v(x) \end{bmatrix} \begin{Bmatrix} \tilde{\mathbf{u}} \\ \tilde{\mathbf{v}} \end{Bmatrix}; & \hat{\boldsymbol{\sigma}}(x) &\cong \mathbf{N}_\sigma \tilde{\boldsymbol{\sigma}} = \begin{bmatrix} \mathbf{N}_{\sigma_x}(x) & \mathbf{0} & \mathbf{0} \\ \mathbf{0} & \mathbf{N}_{\sigma_y}(x) & \mathbf{0} \\ \mathbf{0} & \mathbf{0} & \mathbf{N}_\tau(x) \end{bmatrix} \begin{Bmatrix} \tilde{\boldsymbol{\sigma}}_x \\ \tilde{\boldsymbol{\sigma}}_y \\ \tilde{\boldsymbol{\tau}} \end{Bmatrix}; \\ \hat{\mathbf{s}}'(x) &\cong \mathbf{B}_s \tilde{\mathbf{s}} = \begin{bmatrix} \mathbf{N}'_u(x) & \mathbf{0} \\ \mathbf{0} & \mathbf{N}'_v(x) \end{bmatrix} \begin{Bmatrix} \tilde{\mathbf{u}} \\ \tilde{\mathbf{v}} \end{Bmatrix}; & \hat{\boldsymbol{\sigma}}'(x) &\cong \mathbf{B}_\sigma \tilde{\boldsymbol{\sigma}} = \begin{bmatrix} \mathbf{N}'_{\sigma_x}(x) & \mathbf{0} & \mathbf{0} \\ \mathbf{0} & \mathbf{N}'_{\sigma_y}(x) & \mathbf{0} \\ \mathbf{0} & \mathbf{0} & \mathbf{N}'_\tau(x) \end{bmatrix} \begin{Bmatrix} \tilde{\boldsymbol{\sigma}}_x \\ \tilde{\boldsymbol{\sigma}}_y \\ \tilde{\boldsymbol{\tau}} \end{Bmatrix} \end{aligned} \quad (37)$$

From now on, for the sake of notational simplicity, we will drop the explicit dependency on x for the involved fields.

6.1 Weak problem formulation

We now make explicit the weak formulation we will use as a starting point for the FE discretization. To this end, we first recall the beam model variational formulation (26). Then, we integrate by parts with respect to the x direction both the first and the third terms of Equation (26). We thus obtain:

Find $\hat{\mathbf{s}} \in \widetilde{W}$ and $\hat{\boldsymbol{\sigma}} \in \widetilde{S}$ such that for every $\delta \hat{\mathbf{s}} \in \widetilde{W}$ and for every $\delta \hat{\boldsymbol{\sigma}} \in \widetilde{S}$

$$\delta J_{HR} = \int_l \left(\delta \hat{\mathbf{s}}'^T \mathbf{G}_{s\sigma} \hat{\boldsymbol{\sigma}} - \delta \hat{\mathbf{s}}^T \mathbf{H}_{s\sigma'} \hat{\boldsymbol{\sigma}} + \delta \hat{\boldsymbol{\sigma}}^T \mathbf{G}_{\sigma s} \hat{\mathbf{s}}' - \delta \hat{\boldsymbol{\sigma}}^T \mathbf{H}_{\sigma' s} \hat{\mathbf{s}} - \delta \hat{\boldsymbol{\sigma}}^T \mathbf{H}_{\sigma\sigma} \hat{\boldsymbol{\sigma}} \right) dx - \delta \hat{\mathbf{s}}^T \mathbf{T}_x \Big|_{x=l} = 0 \quad (38)$$

where

$$\widetilde{W} := \{ \hat{\mathbf{s}} \in H^1(l) : \hat{\mathbf{s}}|_{x=0} = \mathbf{0} \}; \quad \widetilde{S} := L^2(l)$$

We may notice that all the derivatives with respect to x are applied to displacement variables, whereas derivatives with respect to y (incorporated into the \mathbf{H} matrices) are applied to cross-section stress vectors. The resulting variational formulation has the following features:

- The obtained weak formulation (38) is symmetric.
- y -derivatives applied to stresses and the essential conditions of S_t^{dd} (cf. Section 3.2.2) most likely lead to a formulation which accurately solve the equilibrium equation in the y direction, i.e. in the cross-section.
- x derivatives applied to displacements and the essential condition in \widetilde{W} most likely lead to a formulation which accurately solve the compatibility equation along the beam axis.

The FE discretization simply follows from the application of (37) into the variational formulation (38). We get:

$$\begin{aligned} \delta J_{HR} = & \int_l \left(\delta \tilde{\mathbf{s}}^T \mathbf{B}_s^T \mathbf{G}_{s\sigma} \mathbf{N}_\sigma \tilde{\boldsymbol{\sigma}} - \delta \tilde{\mathbf{s}}^T \mathbf{N}_s^T \mathbf{H}_{s\sigma'} \mathbf{N}_\sigma \tilde{\boldsymbol{\sigma}} + \delta \tilde{\boldsymbol{\sigma}}^T \mathbf{N}_\sigma^T \mathbf{G}_{\sigma s} \mathbf{B}_s \tilde{\mathbf{s}}' \right) dx + \\ & - \int_l \left(\delta \tilde{\boldsymbol{\sigma}}^T \mathbf{N}_\sigma^T \mathbf{H}_{\sigma' s} \mathbf{N}_s \tilde{\mathbf{s}} + \delta \tilde{\boldsymbol{\sigma}}^T \mathbf{N}_\sigma^T \mathbf{H}_{\sigma\sigma} \mathbf{N}_\sigma \tilde{\boldsymbol{\sigma}} \right) dx - \delta \tilde{\mathbf{s}}^T \mathbf{N}_s^T \mathbf{T}_x \Big|_{x=\bar{l}} = 0 \end{aligned} \quad (39)$$

Collecting unknown coefficients in a vector and requiring to satisfy Equation (39) for all the possible virtual fields we obtain:

$$\begin{bmatrix} \mathbf{0} & \mathbf{K}_{s\sigma} \\ \mathbf{K}_{\sigma s} & \mathbf{K}_{\sigma\sigma} \end{bmatrix} \begin{Bmatrix} \tilde{\mathbf{s}} \\ \tilde{\boldsymbol{\sigma}} \end{Bmatrix} = \begin{Bmatrix} \tilde{\mathbf{T}} \\ \mathbf{0} \end{Bmatrix} \quad (40)$$

where

$$\mathbf{K}_{s\sigma} = \mathbf{K}_{\sigma s}^T = \int_l (\mathbf{B}_s^T \mathbf{G}_{s\sigma} \mathbf{N}_\sigma - \mathbf{N}_s^T \mathbf{H}_{s\sigma'} \mathbf{N}_\sigma) dx \quad \mathbf{K}_{\sigma\sigma} = - \int_l \mathbf{N}_\sigma^T \mathbf{H}_{\sigma\sigma} \mathbf{N}_\sigma dx \quad \tilde{\mathbf{T}} = \mathbf{N}_s^T \mathbf{T}_x \Big|_{x=\bar{l}}$$

In what follows we will focus, for all the involved variables, on the finite element spaces shown in Table 4, where we also recall the profile properties which has led to the multi-layered beam model. For the polynomial degrees and continuity requirements, we here use the same notation as in Section 5.2. Thus, for example, the field v is approximated by means of piecewise cubic polynomials, continuous along the axial direction.

	deg (\mathbf{p}_γ)	y continuity	deg (\mathbf{N}_γ)	x continuity
u	1	C^{-1}	2	C^0
v	2	C^{-1}	3	C^0
σ_x	1	C^{-1}	1	C^{-1}
σ_y	3	C^0	3	C^{-1}
τ	2	C^0	2	C^{-1}

Table 4: Degree and continuity properties of shape functions with respect to y and x directions.

We remark that this choice of the finite element shape functions assures the stability and convergence of the resulting discrete scheme. We also notice that stresses are discontinuous across elements along the x direction, so that it is possible to statically condensate them out at the element level, reducing the dimension of the global stiffness matrix and improving efficiency.

6.2 Multilayered homogeneous beam

We now consider the same three layer homogeneous beam introduced in Section 5.2.1. Together with the clamping condition in A_0 , we assume $\bar{l} = 10\text{mm}$ and the beam to be loaded along A_l by the quadratic shear stress distribution $\mathbf{t}|_{A_l} = [0, 3/2(1 - 4y^2)]^T$ [MPa].

6.2.1 Convergence

In Table 5 we report on the mean value of the transverse displacement along A_l , as obtained by employing the following different procedures:

1. the classical Euler-Bernoulli beam model;
2. the classical Timoshenko beam model;
3. the numerical model under investigation, in which the solution is computed using a mesh of 64 elements;
4. a 2D finite element scheme of the structural analysis program ABAQUS, using a fine regular grid of 3500×350 elements.

Due to the large number of elements used, we consider the latter solution as the reference solution, and we denote with v_{ex} its mean value along A_l .

In Table 5 we also report the following relative error quantity:

$$e_{rel} = \frac{|v - v_{ex}|}{|v_{ex}|} \quad (41)$$

where v is the mean value along A_l computed by the various procedures. We remark that e_{rel} gives an indication of the model accuracy, even though it is not the usual error measure in terms of the natural norms.

Beam theory	$v(10)$	$\text{mm} \cdot 10^{-2}$	e_{rel}	$\cdot 10^{-3}$
Euler-Bernoulli	4.000 000		6.192	
Timoshenko	4.030 000		1.261	
Three-layered mixed FE	4.026 460		0.382	
2D solution	4.024 924		-	

Table 5: Transverse displacements and relative errors of the free-edge of a cantilever ($\bar{l} = 10$ and $h = 1$) obtained by different beam theories.

Table 5 shows the superior performance of the three-layered mixed FE with respect to the other considered 1D models.

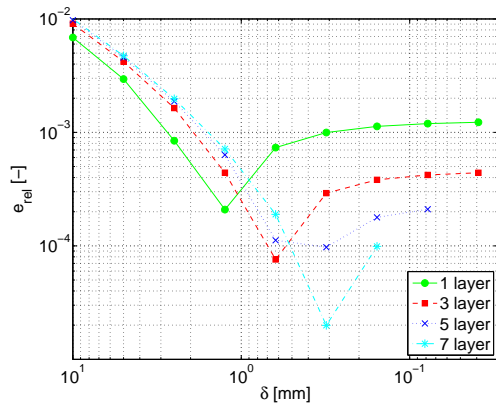
In Figure 3 we study the convergence of our numerical model. More precisely, we plot the relative quantity defined in Equation (41), evaluated considering i layers of thickness $h_i = 1/i$ ($i = 1, 3, 5, 7$), and different mesh sizes δ in the x direction. From Figure 3(a)) we notice that:

- using even a few elements the quantity e_{rel} is under 1%;
- the error e_{rel} decreases as the number of layers increases;
- using highly-refined mesh, the relative error e_{rel} increases, even if it apparently converges to a constant close to 10^{-3} . This behaviour can be explained by recalling that a *modeling error* does necessarily arise. Indeed, the solution of the 2D elastic problem and the one of the multi-layered beam mixed model do differ from each others, for a fixed length and thickness of the beam.

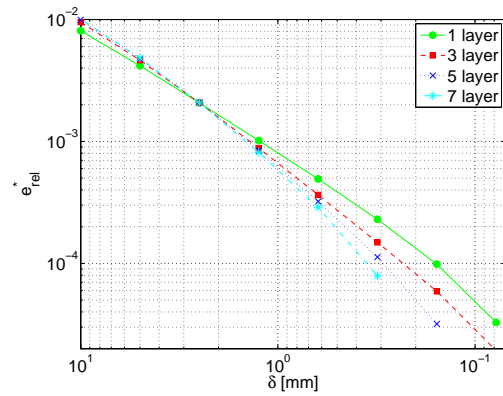
In Figure 3(b) we consider another relative quantity, namely e_{rel}^* . Such a quantity is similar that defined in (41), but here the reference solution is the one obtained by the FE analysis of the multi-layered model using the most refined mesh. We notice that:

- the sequences of errors e_{rel}^* are monotonically convergent to zero;
- fixing the number of layers, the log-log plots of errors suggest a convergence rate of the order of α , with $\alpha \approx 1$.

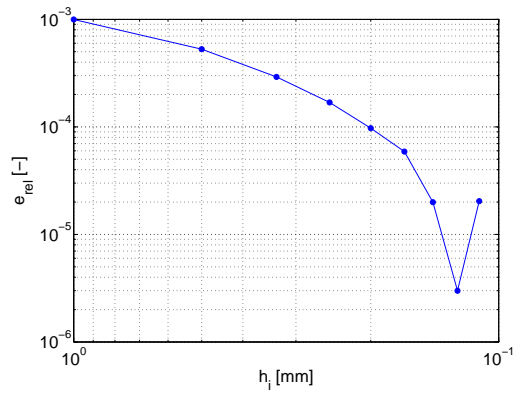
Finally, in Figure 3(c) we plot the relative error e_{rel} versus the number of layers (results obtained using a mesh of 32 elements). It is evident that the relative error decreases incrementing the number of layers even if the succession is not linear.



(a) Relative error e_{rel} , evaluated assuming $v_{ex} = 2D$ numerical solution.



(b) Relative error e_{rel}^* , evaluated assuming $v_{ex} = 1D$ numerical solution obtained using the most refined x -direction mesh.



(c) Relative error, plotted as a function of the layer thickness h_i , with mesh size $\delta = 0.3125\text{mm}$.

Figure 3: Relative errors on free-edge, transverse displacement for different mesh sizes δ and different number of layers.

6.2.2 Boundary effects

As already noticed in Section 5.2.1, the model under investigation is capable to capture some local effect near the clamped boundary; we here present some results focused on that issue. Even though this study is far from being exhaustive, it gives an indication of the model potentials. In what follows the computations are performed using a mesh of 64 elements. To highlight the boundary effects we consider a beam analogous to the one introduced at the beginning of Section 6.2 in which we set $\bar{l} = 2.5\text{mm}$. The results are reported in Figures 4, 5 and 6.

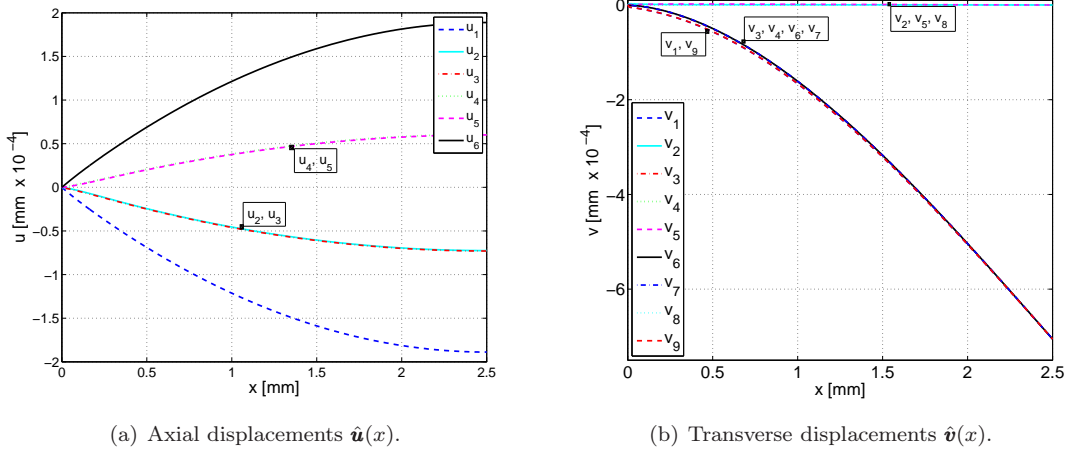


Figure 4: Axial and transverse displacements of a three-layer, homogeneous cantilever, clamped in $x = 0$, loaded at $x = 2.5$ by a quadratic shear distribution and modeled by means of 64 elements.

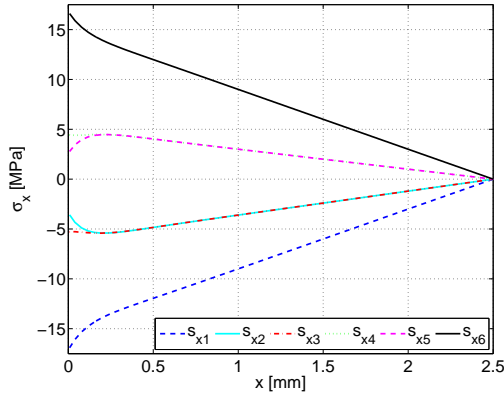


Figure 5: Axial stress $\hat{\sigma}_x(x)$ of a three layer, homogeneous cantilever, clamped in $x = 0$, loaded at $x = 2.5$ by a quadratic shear distribution and modeled with 64 elements.

We can appreciate the following.

- Far from the boundary, it is possible to recognize the classical beam solution (constant shear stress $\tau(x)$, linear axial stress $\sigma_x(x)$, quadratic horizontal displacement $u(x)$ and cubic transverse displacement $v(x)$).
- As expected, the boundary effects decay as a dumped harmonic functions.
- The local effects decay very rapidly, so that only the first oscillation is significant. This result is consistent with the other models capable to capture this kind of boundary effects.

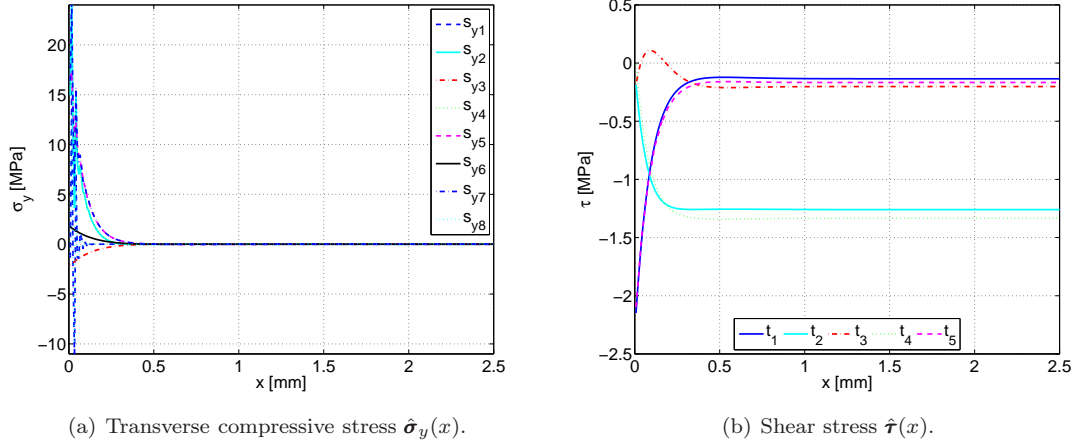


Figure 6: Stresses $\hat{\sigma}_y(x)$ and $\hat{\tau}(x)$ of a three layer, homogeneous cantilever, clamped in $x = 0$, loaded at $x = 2.5$ by a quadratic shear distribution and modeled by means of 64 elements.

- The section striction, described by the displacement quadratic terms v_2 , v_5 and v_8 , is negligible, as assumed in first-order theories.

As specified in Table 4, in the numerical model under discussion we do not *a-priori* impose displacement continuity across layers. In Figure 7 we plot the jump of the displacement field across the inter-layer surfaces S_1 and S_2 . Figure 7(b) highlights that the transverse displacement jump

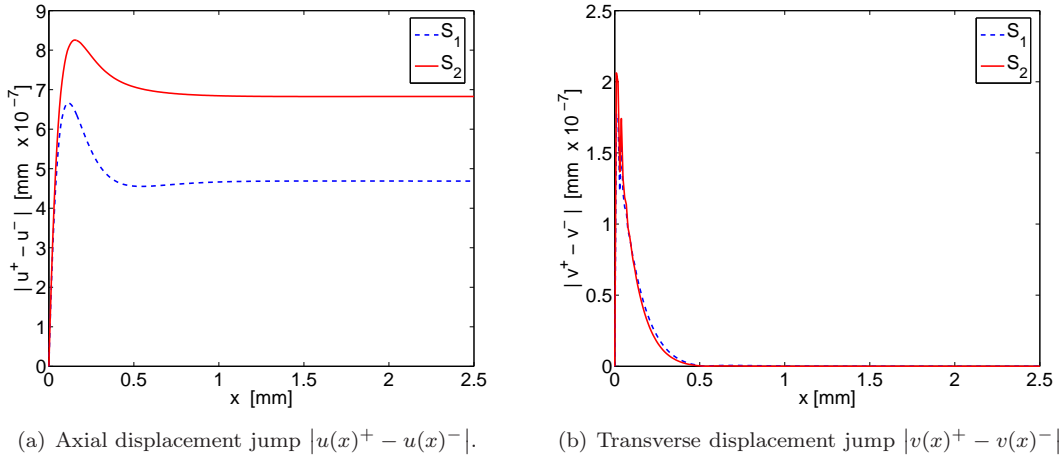


Figure 7: Relative axial and transverse displacements (i.e. compatibility errors) evaluated on interlayer surfaces $S_1 : y = -1/5$ and $S_2 : y = 1/6$.

rapidly decay far from the clamped boundary. On the other hand, from Figure 7(a) we see that, far from the clamped boundary, the axial displacement jump $|u(x)^+ - u(x)^-|$ tends to a value different from zero (of the order of 10^{-7} mm). However, we notice that the displacement field is much greater, since it is of the order of 10^{-4} mm.

6.3 Multilayered non-homogeneous beams

We now consider two non-homogeneous beams. For these cases, we particularly focus on the cross-section stress distributions, since such quantities are only seldom accurately captured in classical beam models.

6.3.1 Symmetric section

We consider a cantilever composed by three layers, clamped in A_0 , for which $\bar{l} = 5\text{mm}$ and $\mathbf{t}|_{A_t} = [0, 3/2(1 - 4y^2)]^T$ [MPa]; geometry and mechanical properties are specified in the following vectors:

$$\mathbf{h} = \begin{Bmatrix} 0.25 \\ 0.50 \\ 0.25 \end{Bmatrix} [\text{mm}] \quad \mathbf{E} = \begin{Bmatrix} 1 \cdot 10^5 \\ 1 \cdot 10^3 \\ 1 \cdot 10^5 \end{Bmatrix} [\text{MPa}] \quad \boldsymbol{\nu} = \begin{Bmatrix} 0.25 \\ 0.25 \\ 0.25 \end{Bmatrix} [-]$$

We evaluate the solution of the 1D model assuming a mesh size $\delta = 0.15625\text{mm}$ (32 elements) and the 2D solution using ABAQUS software and considering a mesh of 200×1000 square elements. For both the models we evaluate the stress distributions at different sections: $x = 2.5$, $x = 0.5$ and $x = 0.125$, as reported in Figures 8, 9 and 10 respectively.

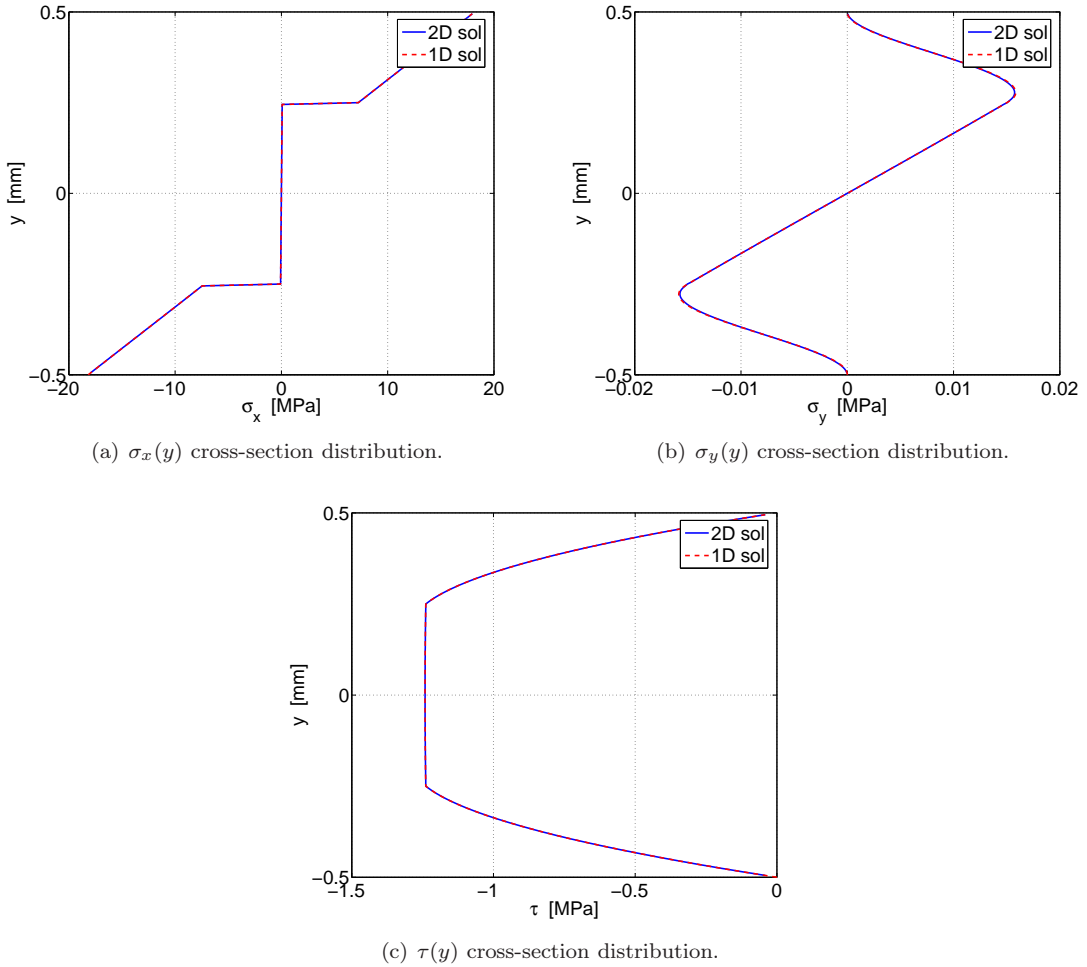


Figure 8: Cross-section stress-distributions evaluated at $x = 2.5$, far from the clamped boundary. 1D and 2D solutions for the symmetric section.

The capability of the numerical model to reproduce a very accurate stress distribution, far from the clamped boundary, is clearly seen from Figures 8. A similar feature is also maintained close the clamped boundary (see Figures 9 and 10), even though some error progressively arises as we approach $x = 0$. In particular, the axial stress σ_x and the shear stress τ are very accurately described, whereas the σ_y approximation exhibit a worse performance (maybe also because some kind of instability arises, cf. Figure 6(a)).

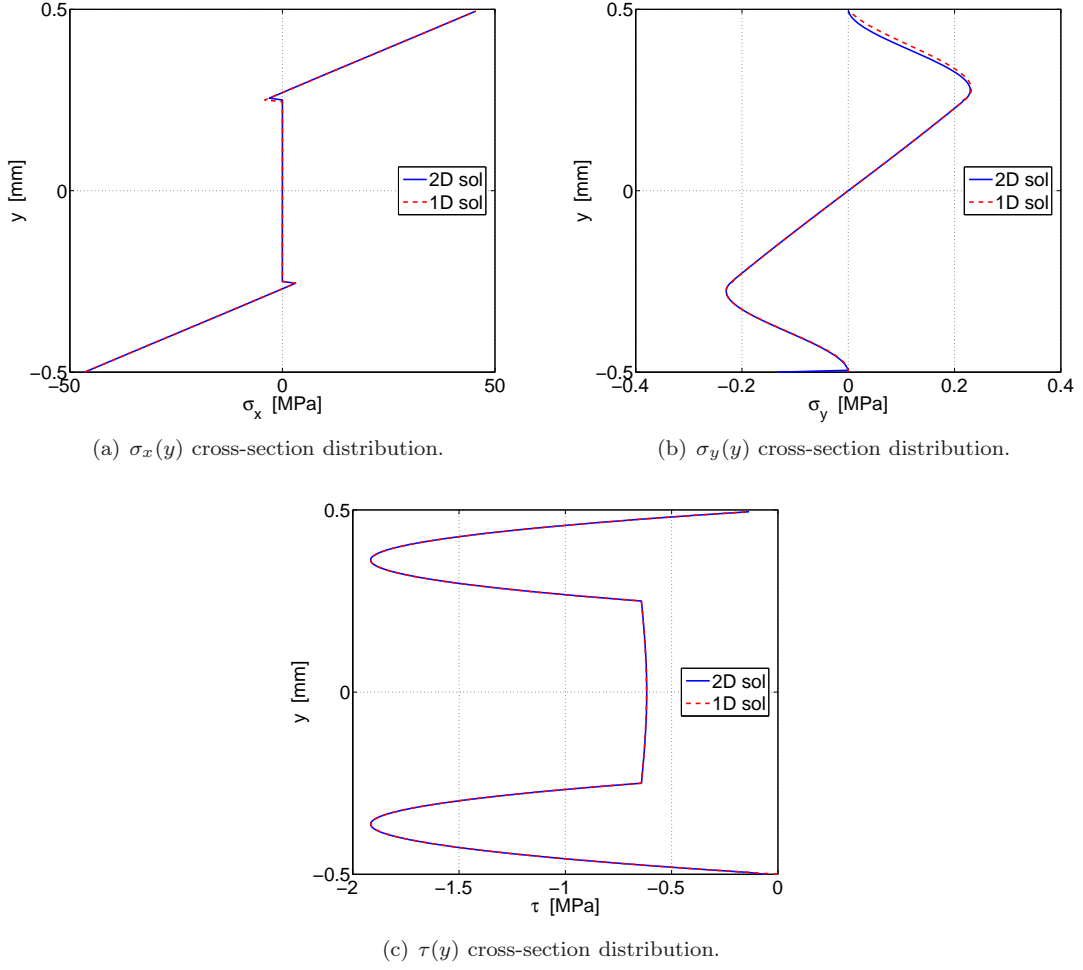


Figure 9: Cross-section stress-distributions evaluated at $x = 0.5$, close to the clamped boundary. 1D and 2D solutions for the symmetric section.

6.3.2 Non-symmetric section

We consider a cantilever composed by four layers, clamped in A_0 , and for which $\bar{l} = 5\text{mm}$. The applied traction is: $\mathbf{t}|_{A_l} = [0, 3/2(1 - 4y^2)]^T$ [MPa]. The geometric and mechanical properties of the section are:

$$\mathbf{h} = \begin{Bmatrix} 0.25 \\ 0.25 \\ 0.25 \\ 0.25 \end{Bmatrix} [\text{mm}] \quad \mathbf{E} = \begin{Bmatrix} 1 \cdot 10^5 \\ 1 \cdot 10^3 \\ 1 \cdot 10^5 \\ 1 \cdot 10^3 \end{Bmatrix} [\text{MPa}] \quad \boldsymbol{\nu} = \begin{Bmatrix} 0.25 \\ 0.25 \\ 0.25 \\ 0.25 \end{Bmatrix} [-]$$

We evaluate the 1D and 2D solutions using the same meshes as for the symmetric case of Section 6.3.1. The computed stress distributions at $x = 2.5$ is reported in Figures 11.

As in the symmetric case, there is no significant difference between the 1D and the 2D cross-section stress distributions. We only notice a small deviation (below 1%) in the plot of the σ_y .

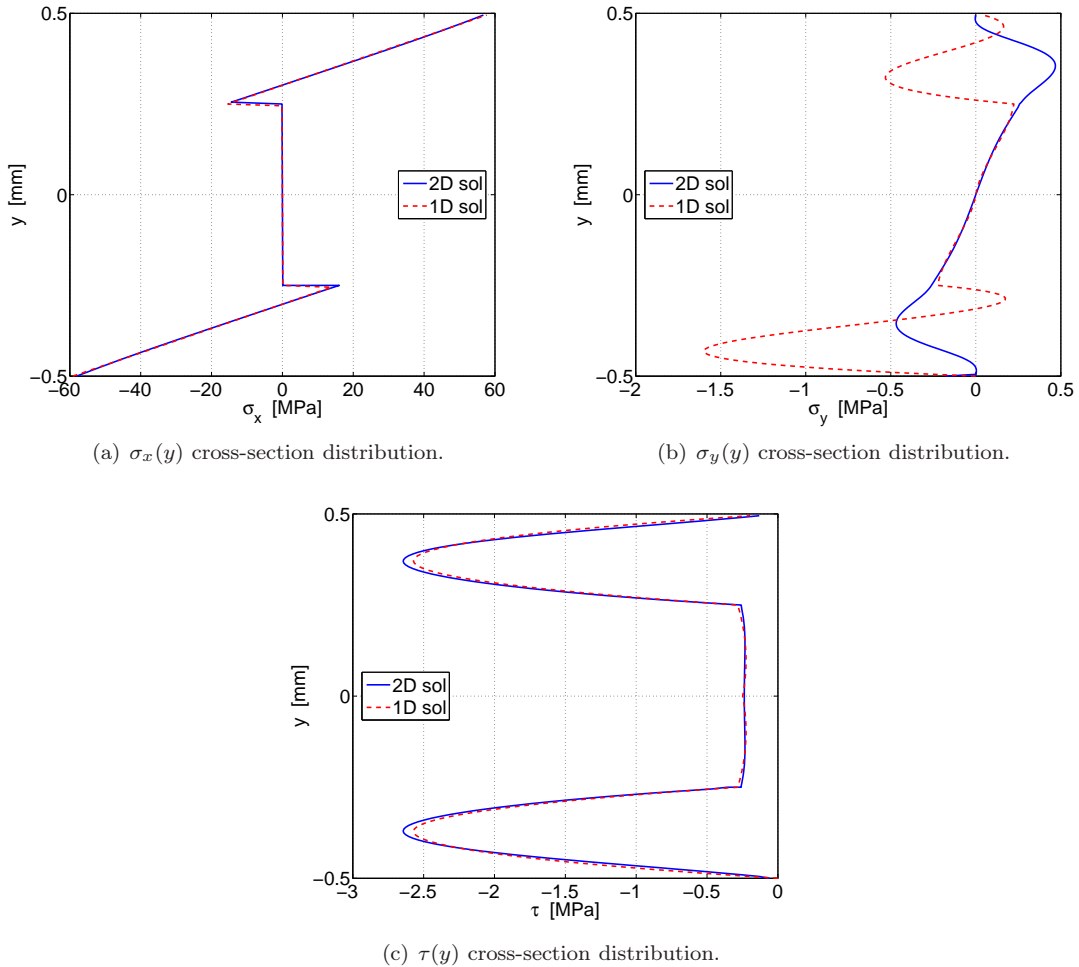


Figure 10: Cross-section stress-distributions evaluated at $x = 0.125$, very close to the clamped boundary. 1D and 2D solutions for the symmetric section.

7 Conclusions

In this paper we developed planar beam models based on a dimension reduction by variational approach. More precisely, we selected a suitable variational formulation among the ones available in the literature. Our choice of the variational principle was motivated by the need to accurately describe the stress profiles. In Sections 4 and 5 we gave the general derivation of the beam models, together with a couple of examples. In Section 6 we focused on the multi-layered model introduced in Section 5, for which we developed an efficient Finite Element scheme, as assessed by the presented numerical results.

Future developments of this work could include 1) the rigorous mathematical study of the models; 2) the generalization to 3D beams with variable cross-section; 3) the treatment of more sophisticated constitutive laws.

Acknowledgments

The authors would like to thank professors Elio Sacco, Alessandro Reali and Giancarlo Sangalli for several helpful suggestions during the completion of this work.

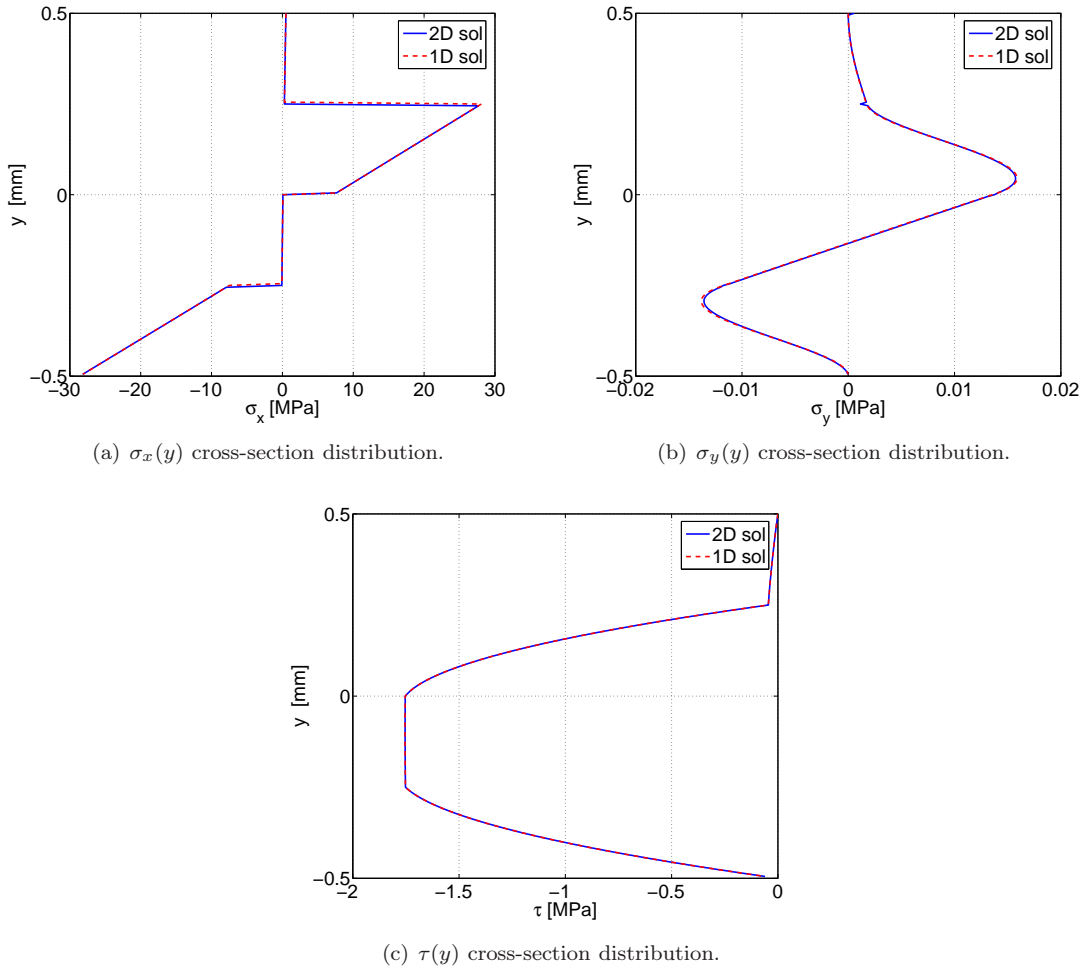


Figure 11: Cross-section stress-distributions evaluated at $x = 2.5$, 1D and 2D solutions for the un-symmetric section.

References

- Alessandrini, S. M., D. N. Arnold, R. S. Falk, and A. L. Madureira (1999). Derivation and justification of plate models by variational methods. *CRM Proceedings and Lecture Notes 21*, 1–20.
- Allix, O. and C. Dupleix-Couderc (2009). A plate theory as a mean to compute precise 3D solutions including edge effects and related issues. *New Trends in Thin Structures*.
- Auricchio, F., C. Lovadina, and A. L. Madureira (2004). An asymptotically optimal model for isotropic heterogeneous linearly elastic plates. *ESAIM Mathematical Modelling and Numerical Analysis 38*, 877–897.
- Auricchio, F. and E. Sacco (1999). A mixed-enhanced finite-element for the analysis of laminated composite plates. *International Journal for Numerical Methods in Engineering 44*, 1481–1504.
- Carrera, E. (2000). Assessment of mixed and classical theories on global and local response of multilayered orthotropic plates. *Composite Structures 50*, 183–198.
- Carrera, E. (2001). Developments, ideas and evaluations based upon Reissner’s mixed variational

- theorem in the modeling of multilayered plates and shells. *Applied Mechanics Review* 54, 301–329.
- Carrera, E. and L. Demasi (2002). Classical and advanced multilayered plate elements based upon PVD and RMVT. Part 1: derivation of finite element matrices. *International Journal for Numerical Methods in Engineering* 55, 191–231.
- Demasi, L. (2009a). Mixed plate theories based on the generalized unified formulation. Part I: governing equations. *Composite Structures* 87, 1–11.
- Demasi, L. (2009b). Mixed plate theories based on the generalized unified formulation. Part II: layerwise theories. *Composite Structures* 87, 12–22.
- Demasi, L. (2009c). Mixed plate theories based on the generalized unified formulation. Part III: advanced mixed high order shear deformation theories. *Composite Structures* 87, 183–194.
- Demasi, L. (2009d). Mixed plate theories based on the generalized unified formulation. Part IV: zig-zag theories. *Composite Structures* 87, 195–205.
- Demasi, L. (2009e). Mixed plate theories based on the generalized unified formulation. Part V: results. *Composite Structures* 88, 1–16.
- Feng, W. and S. Hoa (1998). Partial hybrid finite elements for composite laminates. *Finite Elements in Analysis and Design* 30, 365–382.
- Hjelmstad, K. D. (2005). *Fundamentals of structural mechanics*. Springer.
- Huang, Y., S. Di, C. Wu, and H. Sun (2002). Bending analysis of composite laminated plates using a partially hybrid stress element with interlaminar continuity. *Computers and Structures* 80, 403–410.
- Icardi, U. and A. Atzori (2004). Simple, efficient mixed solid element for accurate analysis of local effects in laminated and sandwich composites. *Advances in Engineering Software* 35, 843–859.
- Ladeveze, P. and J. Simmonds (1998). New concepts for linear beam theory with arbitrary geometry and loading. *European Journal of Mechanics, A/solids* 17, 377–402.
- Lo, K., R. Christensen, and E. Wu (1977a). A high order theory for plate deformations, Part I: homogeneous plates. *Journal of Applied Mechanics* 44, 663–668.
- Lo, K., R. Christensen, and E. Wu (1977b). A high order theory for plate deformations, Part II: laminated plates. *Journal of Applied Mechanics* 44, 669–676.
- Reddy, J. (1984). A simple higher-order theory of laminated composite plates. *ASME, Journal of Applied Mechanics of Composite Materials* 51, 745–752.
- Reissner, E. (1986). On a variational theorem and on shear deformable plate theory. *International Journal for Numerical Methods in Engineering* 23, 193–198.
- Rohwer, K., S. Friedrichs, and C. Wehmeyer (2005). Analyzing laminated structures from fiber - reinforced composite material - an assessment. *Technische Mechanik* 25, 59–79.
- Rohwer, K. and R. Rolfes (1998). Calculating 3D stresses in layered composite plates and shells. *Mechanics of Composite Materials* 34, 355–362.
- Sheinman, I. (2001). On the analytical closed-form solution of high-order kinematic models in laminated beam theory. *International Journal for Numerical Methods in Engineering* 50, 919–936.
- Spilker, R. (1982). Hybrid-stress eight-node elements for thin and thick multilayer laminated plates. *International Journal for Numerical Methods in Engineering* 18, 801–828.

- Timoshenko, S. (1955). Strength of materials. In *Elementary theory and problems*. Krieger publishing company.
- Vinayak, R., G. Prathap, and B. Naganarayana (1996a). Beam elements based on a higher order theory – I formulation and analysis of performance. *Computers and Structures* 58, 775–789.
- Vinayak, R., G. Prathap, and B. Naganarayana (1996b). Beam elements based on a higher order theory – II boundary layer sensitivity and stress oscillations. *Computers and Structures* 58, 791–796.
- Wanji, C. and W. Zhen (2008). A selective review on recent development of displacement-based laminated plate theories. *Recent Patents on Mechanical Engineering* 1, 29–44.